GLOBAL BIOGEOCHEMICAL CYCLES, VOL. 7, NO. 3, PAGES 645-677, SEPTEMBER 1993

# GEOCHEMICAL CYCLES IN AN OCEAN GENERAL CIRCULATION MODEL. PREINDUSTRIAL TRACER DISTRIBUTIONS

Ernst Maier-Reimer
Max Planck-Institut für Meteorologie
Hamburg, Germany

*Abstract.* A state-of-the-art report is given of the Hamburg model of the oceanic carbon cycle. The model advects geochemical tracers important to the carbon cycle by the currents of a general circulation model. The geochemical cycling is driven by a Michaelis - Menten type production kinetics. The model is an extension of the Bacastow and Maier-Reimer (1990) model. It is based on a more realistic current field and includes a mechanism of lysocline - sediment interaction. Principal variables are $\Sigma CO_2$, alkalinity, phosphate, oxygen, and silicate. The carbon variables are defined for $^{12}C$, $^{13}C$, and $^{14}C$ separately. In addition to these carbon isotopes, $^{39}A$ and $\delta^{18}O$ of dissolved oxygen are predicted. The model predicts realistic global patterns of tracer distribution. In the equatorial eastern Pacific, however, the structures are exaggerated due to a strong upwelling which is a common feature of coarse resolution models of the general circulation of the ocean.

## 1. INTRODUCTION

The increase of carbon dioxide in the atmosphere due to the combustion of fossil fuel has stimulated a broad spectrum of research in the past decades [Revelle and Suess, 1957]. At present, it is estimated that approximately one third of the emissions enter the ocean. On the base of existing steady state ocean models, the Intergovernmental Panel on Climate Change (IPCC) gives a most likely value of (2 ± 0.8) GtC/yr for the net air-to-sea flux during the decade 1980-1989 at a total source of (7 ± 1.2) GtC/yr [Houghton et al., 1990]. Recent attempts of a direct estimate from data by use of well calibrated atmospheric transport models give a discrepancy between 0.6 [Tans et al., 1990] and 2.1 GtC/yr [Keeling et al., 1989]. Simplified box models for the sequestering of $CO_2$ by the ocean were developed almost 20 years ago [Oeschger et al., 1975] (see also Bolin [1982]). Traditionally, the fluxes of water between the boxes are calibrated by fitting the results to the distribution of known tracers, primarily radiocarbon. Unfortunately, in this procedure, the calibration using natural radiocarbon gives quite different answers than the calibration using bomb radiocarbon [Siegenthaler, 1983].

With the development of three-dimensional models of the physical circulation of the ocean [Bryan, 1969], the base was given for a treatment of carbon in the sea as a three-dimensional continuum. Maier-Reimer and Hasselmann [1987] studied the uptake of fossil fuel $CO_2$ by the ocean in a purely inorganic model with spatially

Copyright 1993
by the American Geophysical Union

Paper number 93GB01355.
0886-6236/93/93GB-01355$10.00

19449224, 1993, 3, Downloaded from https://agupubs.onlinelibrary.wiley.com/doi/10.1029/93GB01355 by MPI 348 Meteorology, Wiley Online Library on [11/01/2023]. See the Terms and Conditions (https://onlinelibrary.wiley.com/terms-and-conditions) on Wiley Online Library for rules of use; OA articles are governed by the applicable Creative Commons License

homogeneous alkalinity. The main shortcoming of that model (apart from an insufficient formation of North Atlantic deep water) was the complete neglect of any biological processes which are responsible for approximately 80% of the mean gradients of dissolved total $CO_2$ in the ocean [Maier-Reimer and Hasselmann, 1987]. Consequently, the basic state on which the anthropogenic perturbation was imposed, was unrealistic.

A similar approach of three-dimensional modeling has been presented by Sarmiento et al. [1992]. They treated the anthropogenic perturbation of $CO_2$ in the ocean as a perturbation of a basic state, which ignored biological cycling of carbon. In this approach, chemistry appears only in terms of buffer factors which give the transformation of changes in $pCO_2$ to changes in the concentration of dissolved total $CO_2$.

The validation of these simplified three-dimensional models is done primarily by corresponding experiments for radiocarbon [Toggweiler et al., 1989]. A systematic fitting of parameters, as done for box models by simple inversion [cf. Siegenthaler, 1983], is not possible. Since the air to sea exchange of total $CO_2$ is not identical with the exchange of the isotopic composition, a straightforward application of models tuned by radiocarbon to the storage of fossil fuel $CO_2$ imposes some uncertainty.

Najjar [1990] and Najjar et al. [1992] presented a model for the cycling of phosphorus in the Geophysics Fluid Dynamics Laboratory (GFDL) circulation model. They determined the export production from a restoring of the models surface phosphate values to the observed distribution of phosphate. With a plausible release of the production into depth, they obtained reasonable structures of phosphate and oxygen [Sarmiento and Orr, 1991] in the deep ocean within the known weaknesses of the circulation field. In the eastern tropical Pacific and around Antarctica, however, the restoring to surface values invoked an unrealistic high amount of new production.

The need for realistic three-dimensional models of the oceanic carbon cycle is thus widely acknowledged. Entering the decade of the Joint Global Ocean Flux Studies (JGOFS), such models appear to be even more urgently required for the interpretation and dynamical interpolation of the observations. On the other hand, JGOFS will provide an unique dataset for the calibration and validation of such models.

Marine geochemical modeling depends crucially on the assumptions about physical circulation [cf. Siegenthaler, 1983]; on the other hand, physical modelers can gain much insight into their efforts from an inspection of the simulation of geochemical tracers [Maier-Reimer et al., 1993]. In a previous paper [Bacastow and Maier-Reimer, 1990] we presented results based on our state of the art of 1988. The most obvious weakness of that model was the almost complete absence of the Atlantic conveyor belt structure which was most evident in much too high $^{14}C$ age in the Atlantic. In a recent paper [Maier-Reimer et al., 1993] it is pointed out that this weak Atlantic overturning was an effect of inappropriately imposed thermal boundary conditions, rather than an effect of an intrinsic property of the model. In this paper I describe the results of our carbon cycle model embedded in a physical circulation field which fits the ideas about the conveyor belt much better than our previous circulation field. Preliminary results and the model description have been published already in a proceedings volume of a NATO ARW [Maier-Reimer and Bacastow, 1990]. (In that contribution, however, I was too enthusiastic about the ability of a three-dimensional model to produce strong horizontal gradients of the modeled distributions. By an overestimate of the export productivity, the distribution of surface phosphate showed extreme minima of less than one nmol/L, whereas the observations hardly go below 100 nmol/L). The model has been applied in several studies now [e.g. Heinze et al., 1991; Broecker and Maier-Reimer, 1992, Broecker and Maier-Reimer, 1993; Kurz and Maier-Reimer, 1993]. Since a rigorous description has not been published in the open literature, it is repeated here.

Section 2 of this paper gives a comprehensive description of the model. In section 3 the preindustrial tracer distributions are presented rather in the form of an atlas than together with a detailed discussion. Most of the displayed results could be compared directly with observations, but this would almost double the number of figures. The fluxes and the anthropogenic modifications of the system will be discussed in subsequent papers.

19449224, 1993, 3, Downloaded from https://agupubs.onlinelibrary.wiley.com/doi/10.1029/93GB01355 by MPI 348 Meteorology, Wiley Online Library on [11/01/2023]. See the Terms and Conditions (https://onlinelibrary.wiley.com/terms-and-conditions) on Wiley Online Library for rules of use; OA articles are governed by the applicable Creative Commons License

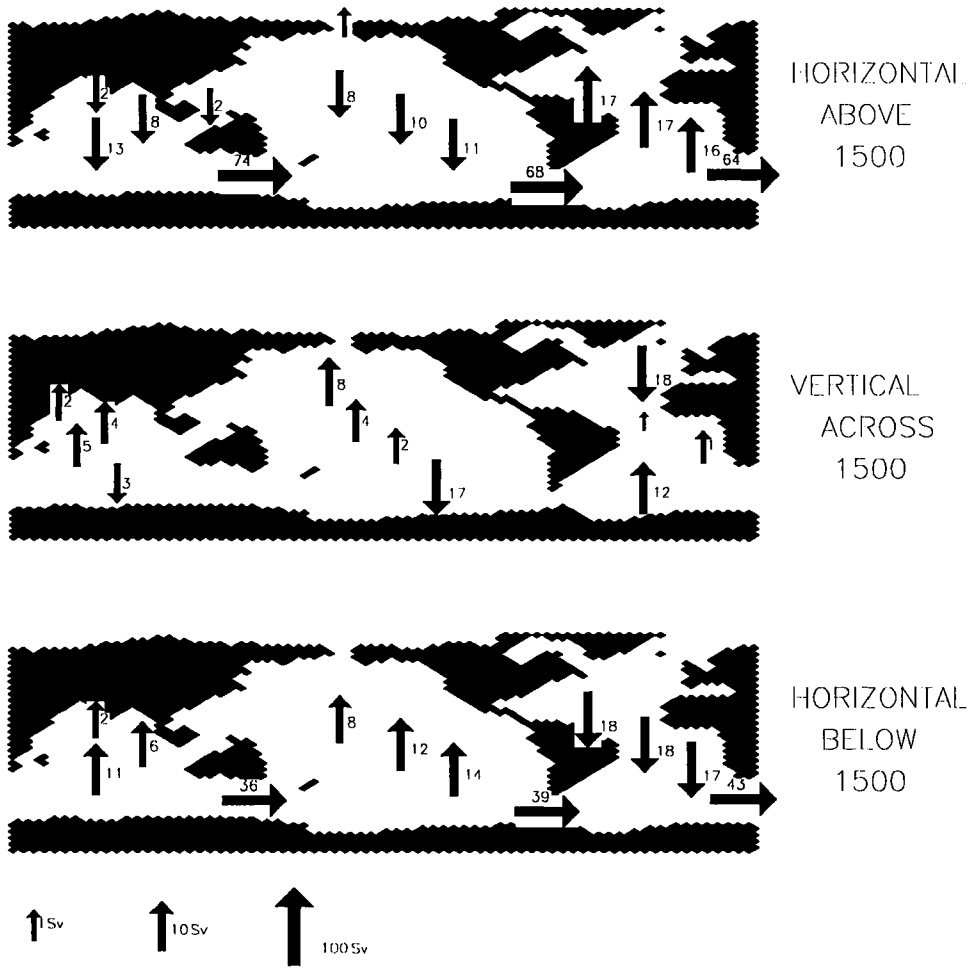


Fig. 1a. The model "Conveyor Belt." Transports are between "boxes" confined at 10 N, 10 S, 40 S, 100 W, 30 E, 140 E, and 1.5 km depth.

## 2. THE MODEL

The model is based on a 15 layer version of the Hamburg Large Scale Geostrophic Ocean General Circulation Model (LSG OGCM) [Maier-Reimer et al., 1993]. The layers are confined by the horizons at 50, 100, 150, 200, 250, 320, 400, 525, 700, 900, 1500, 2500, 3500, and 4500 m. Near the seafloor the spacing is variable in order to allow for a smooth representation of topographic gradients. The main difference to the circulation field of Bacastow and Maier-Reimer lies in the incorporation of a simple sea-ice model which is driven by the Comprehensive Ocean Atmosphere Data Set (COADS) [Woodruff et al., 1987] of atmospheric temperature. The freshwater fluxes were obtained by restoring the model's surface salinity to observations [Levitus, 1982] with a time constant of 2 months. The main difference in the resulting current field is a vigorous outflow of 17 Sv of North Atlantic Deep Water (NADW) at 30°S which did not exist in our earlier studies. Figure 1a displays the structure of the model's global conveyor characteristics.

The carbon cycle model is an extension of the Bacastow and Maier-Reimer [1990] model. It uses the monthly circulation fields of the OGCM and the same time step of one month is taken for the integration of all processes involved. It follows closely generally accepted ideas of primary productivity and fluxes as summarized, for example, in the introductory chapter in the book *Tracers in the Sea* [Broecker and Peng,

19449224, 1993, 3, Downloaded from https://agupubs.onlinelibrary.wiley.com/doi/10.1029/93GB01355 by MPI 348 Meteorology, Wiley Online Library on [11/01/2023]. See the Terms and Conditions (https://onlinelibrary.wiley.com/terms-and-conditions) on Wiley Online Library for rules of use; OA articles are governed by the applicable Creative Commons License

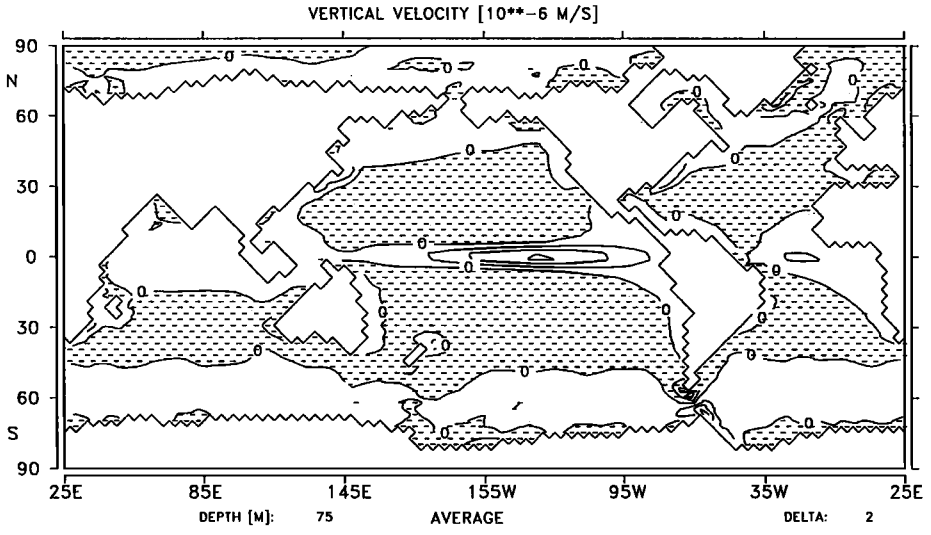


Fig. 1b. Vertical component of velocity at the base of the model's top layer (50 m).

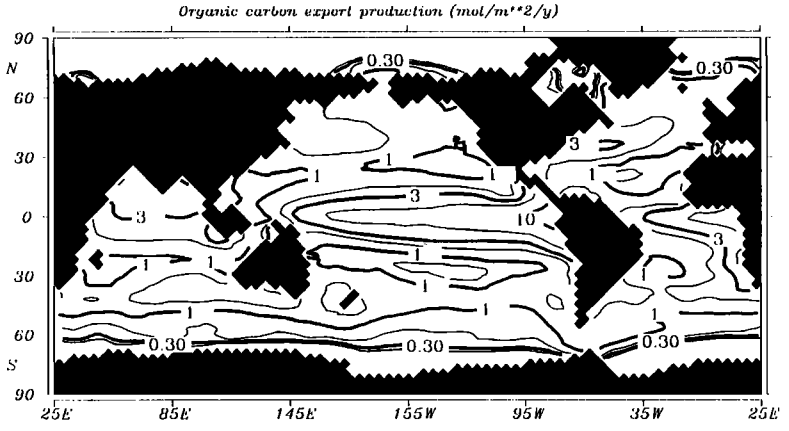


Fig. 1c. Annual mean production of soft tissue.

1982]. The model, as described here, has shortcomings in most of its components. The formulation of plankton productivity is much simpler than in special models of plankton growth [e.g. Dugdale 1967; Radach and Maier-Reimer 1975; Fasham et al., 1990]. Similarly, elaborate models have been developed for the dynamics of sediment deposits [Archer, 1991]. The model is conceptually not a model of biology in the ocean but rather a model of biogenically induced chemical fluxes in the ocean. It is based on the assumption of perfect stoichiometric constancy of organic material. Consequently, we do not address the question of which nutrient really limits the production. We assume one limiting nutrient $PO_4^{3-}$ with a phosphorus to carbon Redfield ratio of 1:122 [Takahashi et al., 1985]. By this choice, the complicated interactions between different components of the nitrogen cycle are disregarded. In this paper, I do not give a complete description of the processes which motivate the formulation of the model details. I assume that the readers of this journal are familiar with these processes and the related notation.

The model has undergone several modifications and extensions during the past years. Since it is not thought to be now in a final state, a more rigorous nomenclature for the different versions may serve to reduce the confusion of future readers. I call the model as presented here HAMOCC 3 (Hamburg model of ocean carbon

19449224, 1993, 3, Downloaded from https://agupubs.onlinelibrary.wiley.com/doi/10.1029/93GB01355 by MPI 348 Meteorology, Wiley Online Library on [11/01/2023]. See the Terms and Conditions (https://onlinelibrary.wiley.com/terms-and-conditions) on Wiley Online Library for rules of use; OA articles are governed by the applicable Creative Commons License

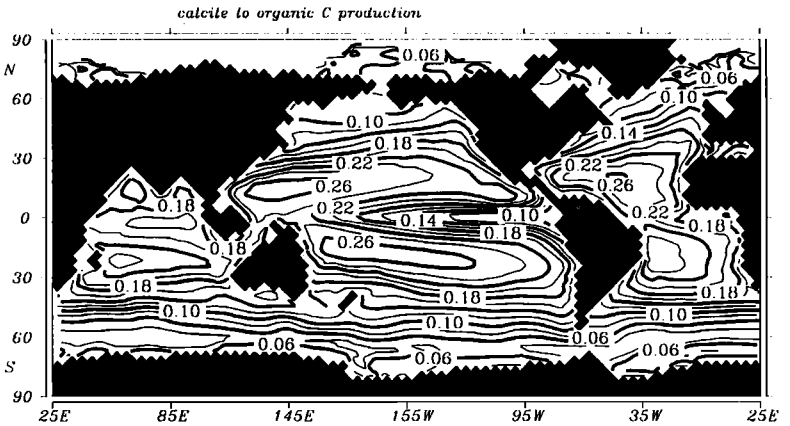


Fig. 1d. Annual mean $C_{carb}:C_{org}$ ratio of export production.

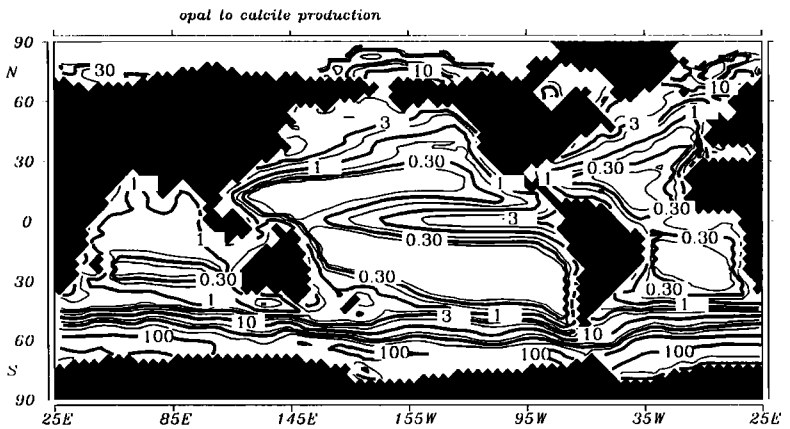


Fig. 1e. Annual mean opal:calcite ratio of export production. The relative maximum along the coast of Southern America and Africa is an artefact from the low ventilation of these semienclosed grid points.

cycle - cycle 3). In this terminology, the Bacastow and Maier-Reimer [1990] model is named HAMOCC 1, and the Heinze et al. [1991] model is HAMOCC 2.

Prognostic variables of the model are in the

Atmosphere

$^{12}CO_2$, $^{13}CO_2$, $^{14}CO_2$, $^{16}O_2$, and $^{18}O_2$

Ocean

$\Sigma^{12}CO_2$, $\Sigma^{13}CO_2$, $\Sigma^{14}CO_2$, $PO^{12}C$, $PO^{13}C$, $PO^{14}C$, $Ca^{12}CO_3$, $Ca^{13}CO_3$, $Ca^{14}CO_3$, alkalinity, phosphate, $^{16}O$, $^{18}O$, silicate, and $^{39}Ar$,

and at the seafloor sediment layers of $CaCO_3$ and organic material, both for all three carbon isotopes.

The isotopes of carbon and oxygen are treated as individual tracers with units of ppm, mol/L, and mol/$m^2$ for the three domains of definition. In any process in which fractionation occurs, the reaction rates dC and dO are determined by $^{12}C$ and $^{18}O$. The variation of $^{13}C$, for instance with fractionation factor F, is then written:

$$d^{13}C = F\, d^{12}C\, (^{13}C/\, ^{12}C)$$

The transformation to the usual $\delta$ and $\Delta$ notations is performed just for the analysis of the results. The absolute values of the isotopic concentrations have no influence on the model's dynamics. Realistic estimates from observations for the inventories of the less abundant isotopes may be introduced, too, for the model diagnostic. The standard sample for

19449224, 1993, 3, Downloaded from https://agupubs.onlinelibrary.wiley.com/doi/10.1029/93GB01355 by MPI 348 Meteorology, Wiley Online Library on [11/01/2023]. See the Terms and Conditions (https://onlinelibrary.wiley.com/terms-and-conditions) on Wiley Online Library for rules of use; OA articles are governed by the applicable Creative Commons License

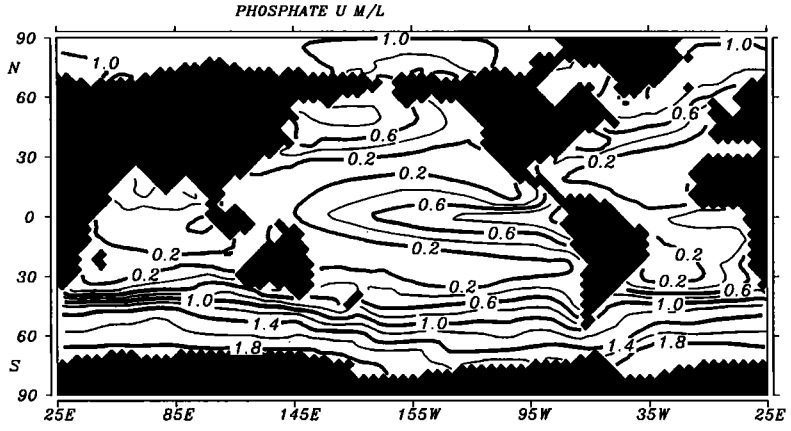


Fig. 2a. Annual mean surface phosphate.

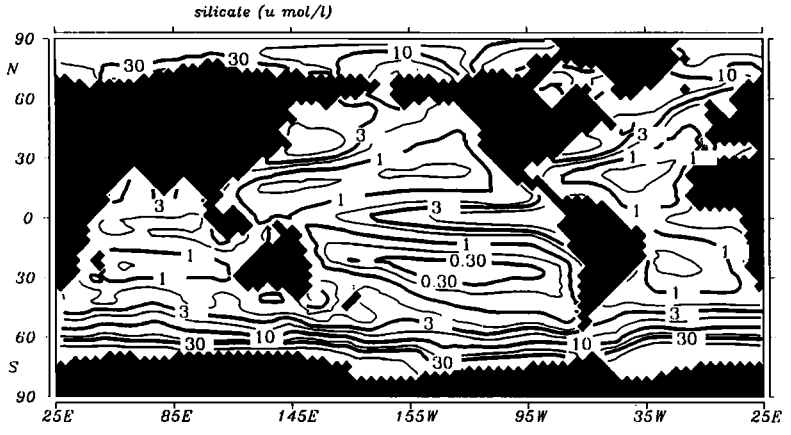


Fig. 2b. Annual mean surface silicate. Lines are drawn at 1, 2, 3, 5, 10, 20, and 50 μ mol/L.

the geochemical notation is computed from the definition that the model should exhibit in the preindustrial stationary state an atmospheric $\delta^{13}C$ of - 6.5%. and zero $\Delta^{14}C$.

In all processes where POC is involved, a constant Redfield ratio is assumed [Takahashi et al., 1985]:

p : N : C : $\Delta O_2$ = 1 : 16 : 122 : -177

(Nitrogen is not treated as separate tracer, but we take into account the modifications of alkalinity exerted by the incorporation of nitrogen into soft tissue.)

The model alkalinity is a simplified form of the exact definition [Dickson, 1981]. It contains the components of the aqueous, carbon, and borate systems only, where total borate is assumed to vary linearly with salinity; it does not appear as an individual tracer. The partitioning between the different states of dissociation, and, thus, its contribution to the total alkalinity, follows from the law of mass action for the boron atoms and for the carbon atoms. The dissociation constants for carbonic acid are taken from Goyet and Poisson [1989], while those for boric acid are from Culberson and Pytkowicz [1968]. The solubility product for calcium carbonate is from Broecker and Takahashi [1978] after Edmond and Gieskes [1970]. The $pCO_2$ of seawater is computed locally from alkalinity and $\Sigma CO_2$, using the formulae for solubility [Weiss, 1974] and the dissociation coefficients. The exact values of the dissociation constants are still in debate. Any systematic error in the coefficients would reflect errors in the $pCO_2$ - $\Sigma CO_2$ - alkalinity system. An inspection of the results of the model, however, indicates that the uncertainties of the coefficients are not crucial. Sarmiento et al. [1992] reported

19449224, 1993, 3, Downloaded from https://agupubs.onlinelibrary.wiley.com/doi/10.1029/93GB01355 by MPI 348 Meteorology, Wiley Online Library on [11/01/2023]. See the Terms and Conditions (https://onlinelibrary.wiley.com/terms-and-conditions) on Wiley Online Library for rules of use; OA articles are governed by the applicable Creative Commons License

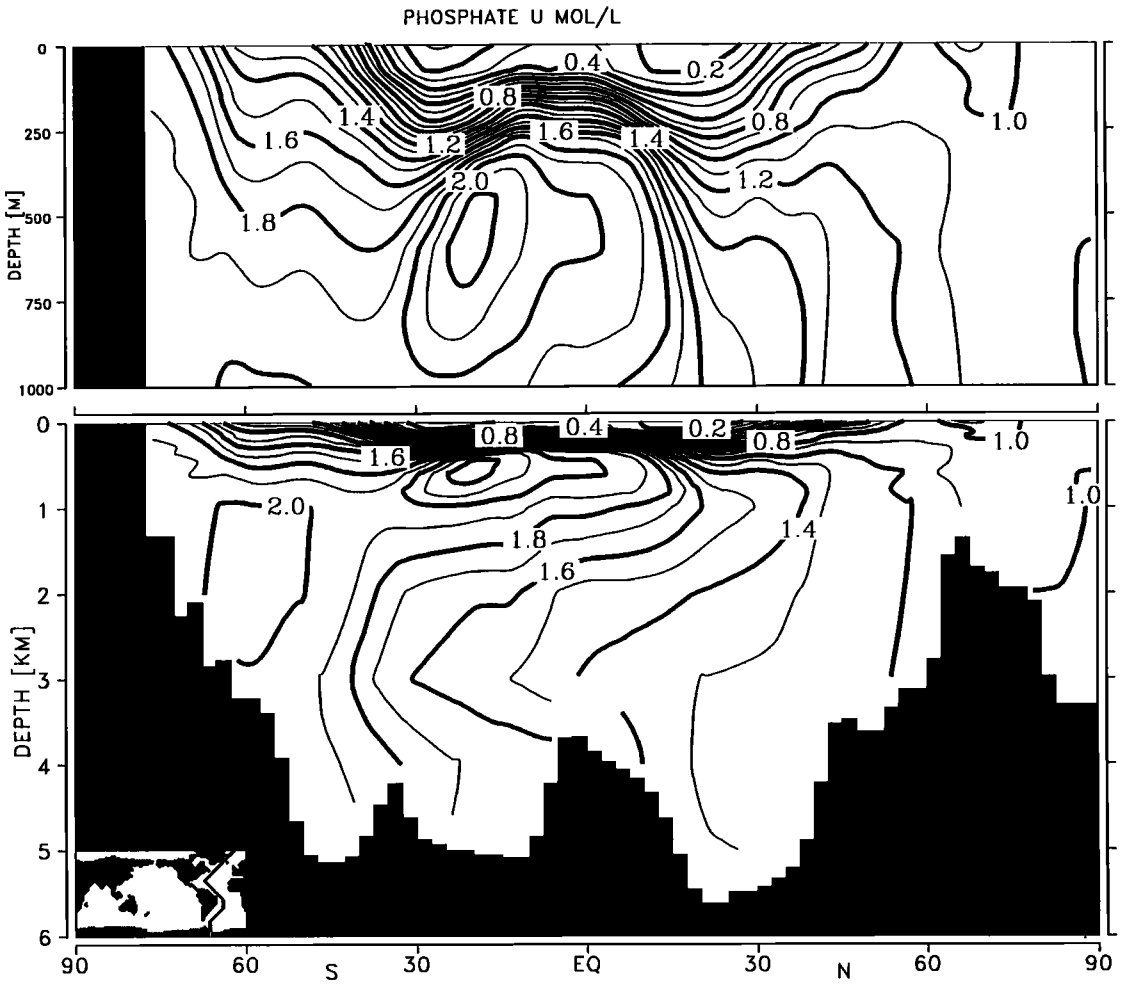


Fig. 3a. Phosphate along a section in the Western Atlantic.

preliminary experiments with different formulations of the coefficients. They found that at least for the problem of $CO_2$ uptake the details do not matter. The position of the lysocline, however, reacts more sensitively on the details of the functional representation of the constants. The discussion emphasizes the global gradients rather than the exact position of the horizon of 100.0 % of saturation.

The role of dissolved organic carbon (DOC) in the marine biota cycle is still controversial. The high radiocarbon age of the "classical" DOC [Williams and Druffel, 1987] indicates that it is not strongly involved. The "new" DOC [Sugimura and Suzuki, 1988] with a much bigger and faster recycling pool was never generally accepted and was questioned recently by Suzuki [1993] himself. It has been demonstrated [Bacastow and Maier-Reimer, 1991; Najjar et al., 1992] that the assumption of a big DOC pool with a life time of the order of a century may serve to remove some apparent flaws of carbon cycle models, especially the high subsurface maximum of phosphate in the eastern Equatorial Pacific. In the model as described here, DOC is not included.

Formally, the model is characterized by a set of differential equations:

$$\frac{\partial C_i}{\partial t} + \underline{V}\nabla C_i - DC_i = \lambda_i C_i + \sum_k F_{ik}(C_i, C_k)$$

where $C_i$ stands for any of the tracers, $\underline{V}$ is the vector of the advection velocity, D denotes the diffusion operator, $\lambda$ denotes tracer specific sink/source terms like decay of $^{14}C$, and F denotes the nonlinear interaction functionals between the

19449224, 1993, 3, Downloaded from https://agupubs.onlinelibrary.wiley.com/doi/10.1029/93GB01355 by MPI 348 Meteorology, Wiley Online Library on [11/01/2023]. See the Terms and Conditions (https://onlinelibrary.wiley.com/terms-and-conditions) on Wiley Online Library for rules of use; OA articles are governed by the applicable Creative Commons License

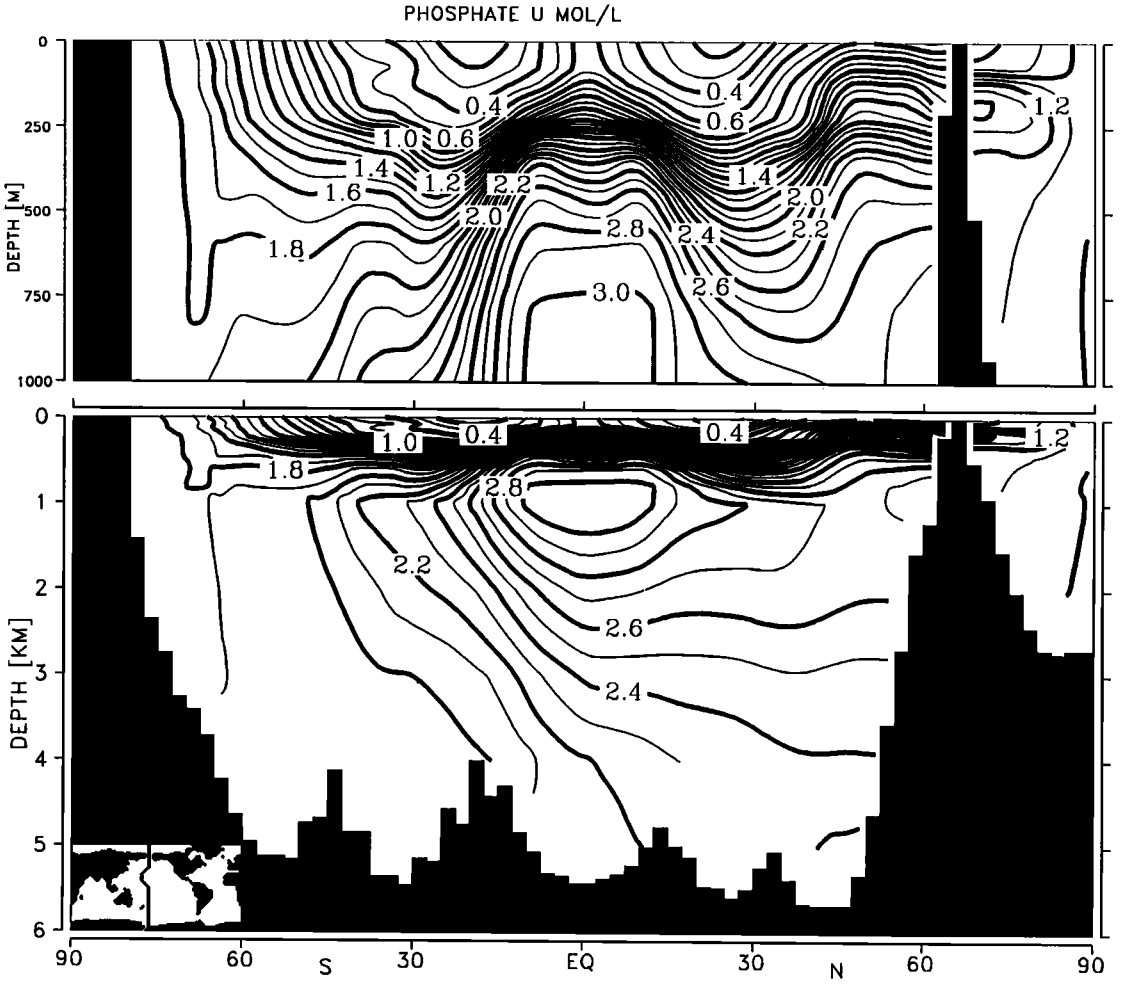


Fig. 3b. Phosphate along a section in the Western Pacific.

tracers. We impose zero fluxes across all boundaries for all tracers but oxygen and the carbon isotopes which are subject to exchange with the atmospheric variables. For all bio-related tracers we do not assume any restoring to observed values. Consequently, the comparison of the tracer fields with observations gives an evaluation of the physical model as well as of the geochemical model.

The formulation of the biogeochemical processes is not straight- forward; the available data do not allow a unique determination of functional relationships with precisely known numbers. In most processes we assume a parameter of maximum interaction which is reduced by limiting factors of the environment. The validation of the model assumptions is done indirectly by comparison of the model tracer distributions with observations, primarily from GEOSECS [Craig et al., 1981; Bainbridge, 1980]. Since the measured distributions represent an integral over many processes acting over a long time, the validation holds only for the whole model, not for any individual process formulation.

### Gas Exchange

The Liss and Merlivat [1986] parametrization, which is primarily dependent on the wind speed, is inconsistent in the global average with the mean gas exchange coefficient derived from the inventories of bomb produced radiocarbon in the ocean [Broecker et al., 1985]. For the experiment described in this paper, a geographically uniform value k =0.06 mol/($m^2$a $\mu$ atm) was chosen, matching the estimate of Broecker et al. [1985]. The appropriate combination of k with the solubility and the buffer factor determines

19449224, 1993, 3, Downloaded from https://agupubs.onlinelibrary.wiley.com/doi/10.1029/93GB01355 by MPI 348 Meteorology, Wiley Online Library on [11/01/2023]. See the Terms and Conditions (https://onlinelibrary.wiley.com/terms-and-conditions) on Wiley Online Library for rules of use; OA articles are governed by the applicable Creative Commons License

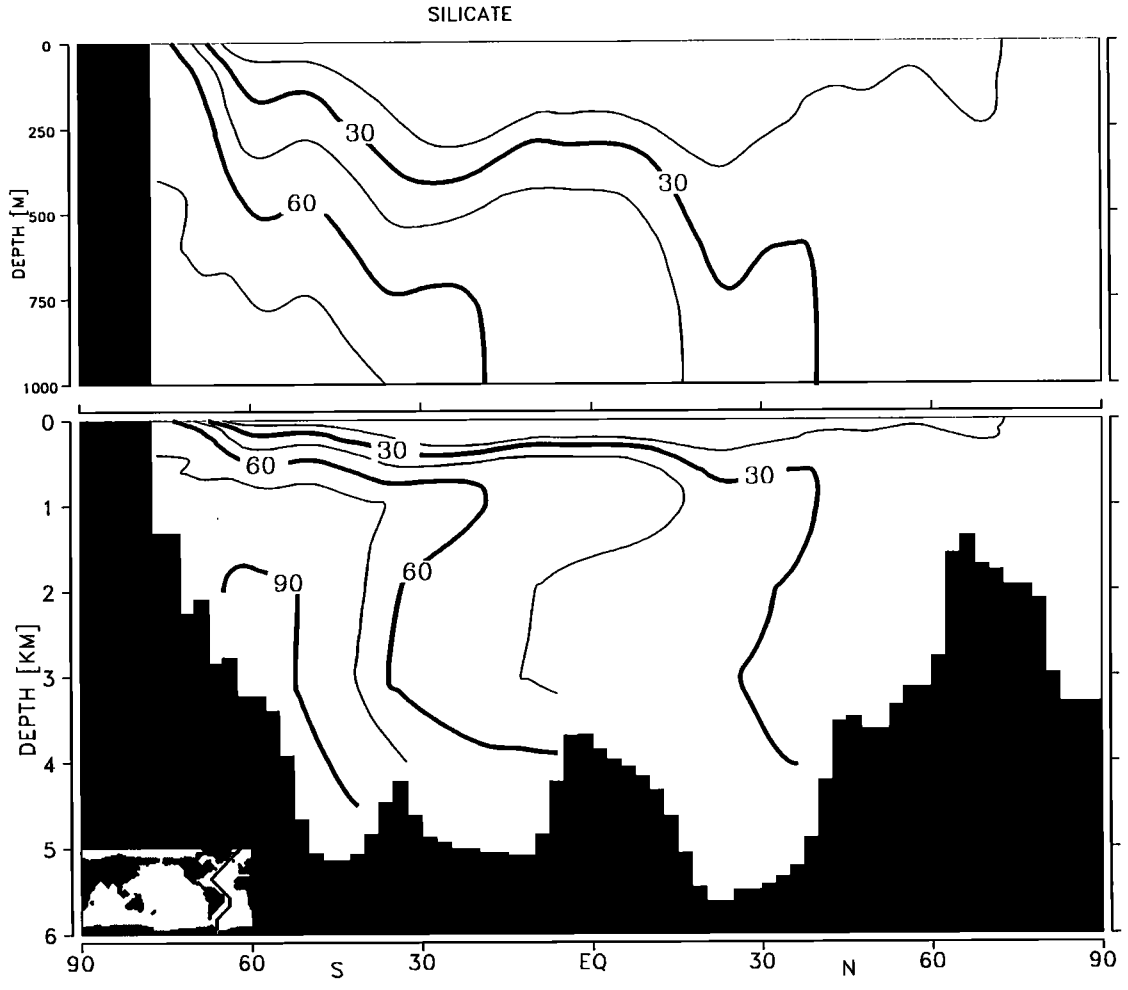


Fig. 3c. Silicate along s dection in the Western Atlantic.

a piston velocity of approximately 100 m/yr. With a time step of one month and a top layer thickness of 50 m, the details of the discretization in time are, consequently, not crucial. The circulation model has on top a simplified sea ice model which does not contain compactness as a variable. For the gas exchange a threshold value of 50 cm of thickness is defined above which the flux is blocked. Between zero and 50 cm of thickness, the gas exchange is linearly reduced to reach zero at 50 cm.

The fractionation of the carbon isotopes stems from a lower tendency of the heavier isotopes to evaporate [Mook et al., 1974]:

$$F^{13}/F^{12} = (1.02389 - 9.483/ T_{abs}),$$

and

$$F^{14}/F^{12} = (F^{13}/F^{12})^2$$

where $T_{abs}$ is the SST in K.

For oxygen, the gas exchange operates an order of magnitude quicker than for $CO_2$, due to the buffering in the $CO_2$-system; we assume the surface oxygen to equilibrate completely at the temperature dependent saturation level within the time step of one month.

*New Production*

Depending on the phosphate concentration P, the new production NP of phosphorus in soft tissue material is written:

$$NP = r\ P\ (\ P/(P + Po))$$

The bracketted term provides a lower productivity rate in nutrient poor water (Michaelis-Menten kinetics, according Dugdale [1967]). We set Po = 0.02 μmol/L

19449224, 1993, 3, Downloaded from https://agupubs.onlinelibrary.wiley.com/doi/10.1029/93GB01355 by MPI 348 Meteorology, Wiley Online Library on [11/01/2023]. See the Terms and Conditions (https://onlinelibrary.wiley.com/terms-and-conditions) on Wiley Online Library for rules of use; OA articles are governed by the applicable Creative Commons License

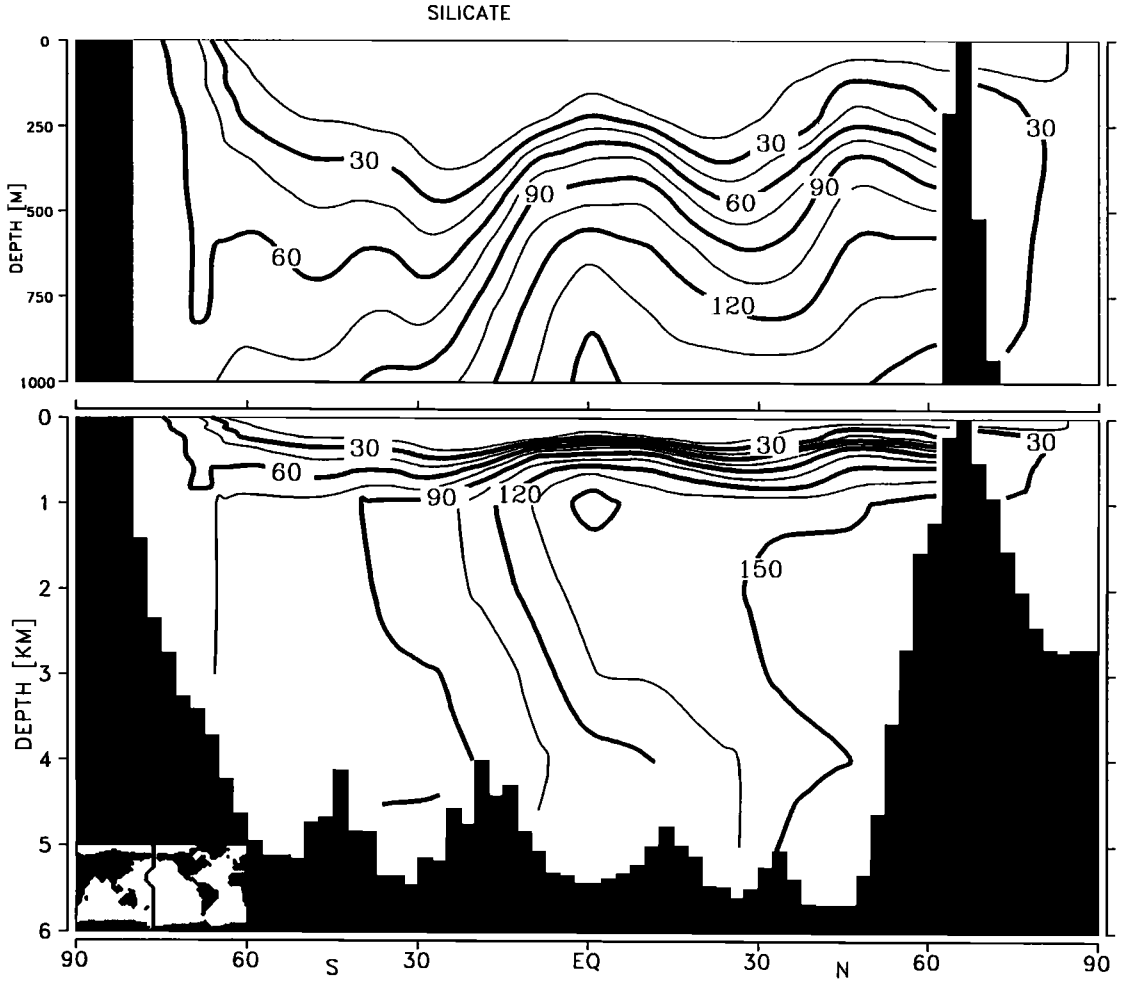


Fig. 3d. Silicate along a section in the Western Pacific.

corresponding to the half-saturation values for nitrate given by Eppley et al. [1969]. The productivity rate r depends on the temperature T (in centigrade), the incoming radiation I as computed by the integration of cos(Δ) (Δ is the solar angle) over the length of day, normalized to a maximum value of unity (ignoring cloudiness), and the actual depth of the mixed layer as represented in the model by the depth Cc of the convective column:

$$r = ro\ I\ (50m/\ Cc)\ (T+2)/(T+10).$$

As mentioned above, the model distributions depend strongly on the choice of ro. With ro = 0.25 $month^{-1}$ we get a realistic simulation of surface phosphate.

We did not assume any kind of iron limitation as proposed by several authors [e.g., Martin et al., 1990].

NP effects a transformation from P and $\Sigma CO_2$ to the pool of particulate organic carbon (POC). The alkalinity is increased by 16 NP due to the incorporation of nitrate into soft tissue. An inspection of phosphate versus $\delta^{13}C$ scatter diagrams [Broecker and Peng, 1982] in the deep ocean indicates that for the implementation of carbon into plant material, the fractionation Fp of heavy carbon isotopes should be proportional to 0.98 times the local isotopic ratios of $^{13}C$ and, consequently, 0.9604 for $^{14}C$, in $\Sigma CO_2$.

The newly formed POC quantities are released instantaneously in the depth z according a penetration flux $(100\ m\ /\ z)^{0.8}$ for z > 100 m (Berger et al. [1987] based on Suess [1980]. The flux reaching the bottom is added to an organic sediment layer where remineralization occurs with a time constant of 10 months. In the

19449224, 1993, 3, Downloaded from https://agupubs.onlinelibrary.wiley.com/doi/10.1029/93GB01355 by MPI 348 Meteorology, Wiley Online Library on [11/01/2023]. See the Terms and Conditions (https://onlinelibrary.wiley.com/terms-and-conditions) on Wiley Online Library for rules of use; OA articles are governed by the applicable Creative Commons License

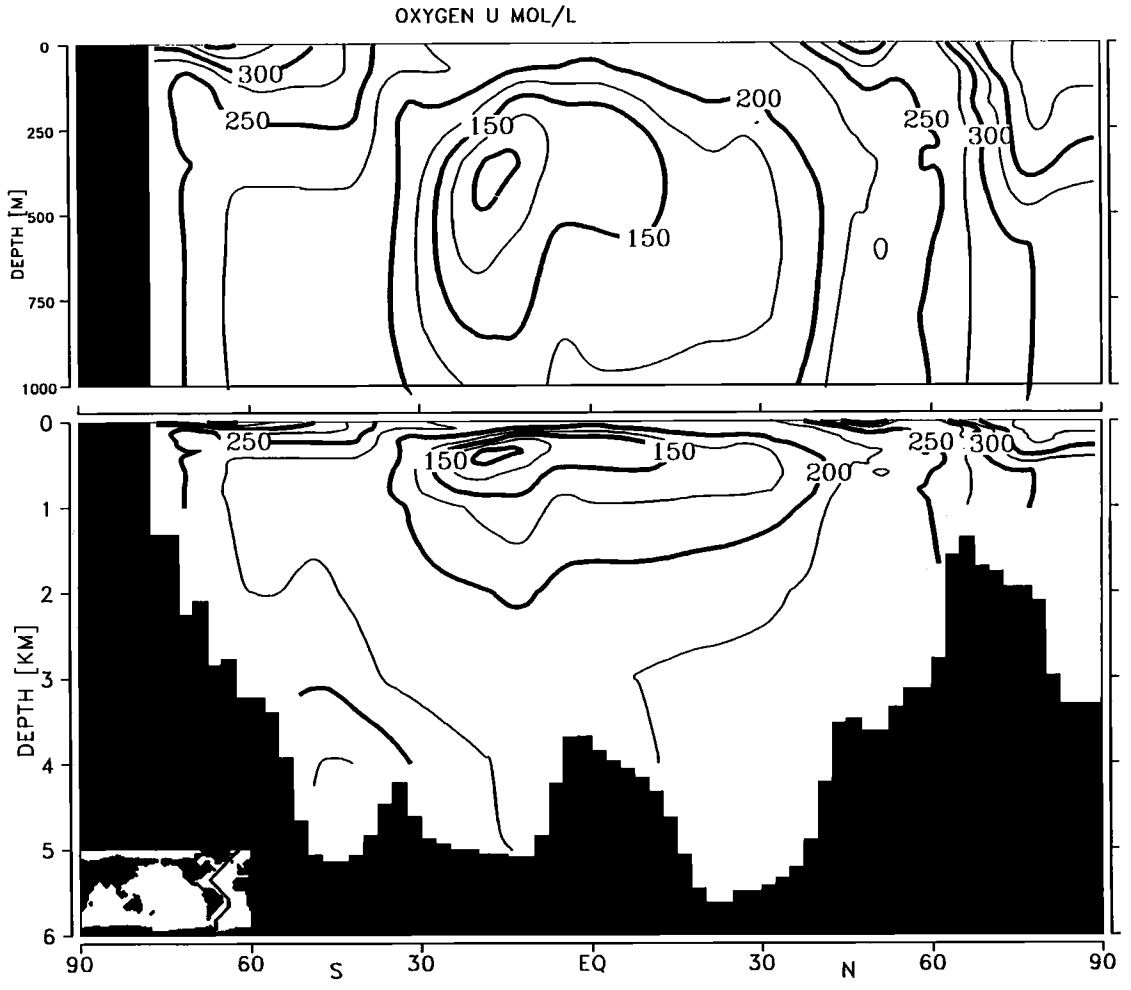


Fig. 4a. Oxygen along a section in the Western Atlantic.

experiment described here, the organic sediment pool is less than 15 G; for the global carbon budget, this is only a marginal pool.

*Shell Material*

We assume silicate to be the preferred concrete to build shells. The data show a much stronger depletion of silicate in surface waters than of phosphate or nitrate. This feature is simulated by a greater penetration depth of silicate material and by a stronger utilization rate. The latter can be interpreted as a cumulative effect of preferential diatom blooms and of the assumption that the export of silicate shells is connected with the gross primary productivity rather than with the new production, the main process of our model. With a (rather arbitrarily chosen) constant relation of 1:10 between P and Si utilization we define a potential for silicate production

$$PSi = \min(Si, 600\ NP)\ Si/(Si+Sio).$$

(note that the global inventory of Si is 60 times higher than of P). Sio is set to 4 μmol/L.

The formation of carbonate shells is reduced in low-temperature regions [cf. Lisitzin, 1971; Dymond and Lyle, 1985; Tsunogai and Noriki, 1991]. We define a potential for carbonate formation

$$PCO_3 = 61NP\exp(0.1(T-10))/1+\exp(0.1(T-10)))$$

The temperature factor is approximately one at temperatures above 20°C and goes to zero as the temperature approaches the freezing point. The factor 61 is half the C:P

19449224, 1993, 3, Downloaded from https://agupubs.onlinelibrary.wiley.com/doi/10.1029/93GB01355 by MPI 348 Meteorology, Wiley Online Library on [11/01/2023]. See the Terms and Conditions (https://onlinelibrary.wiley.com/terms-and-conditions) on Wiley Online Library for rules of use; OA articles are governed by the applicable Creative Commons License

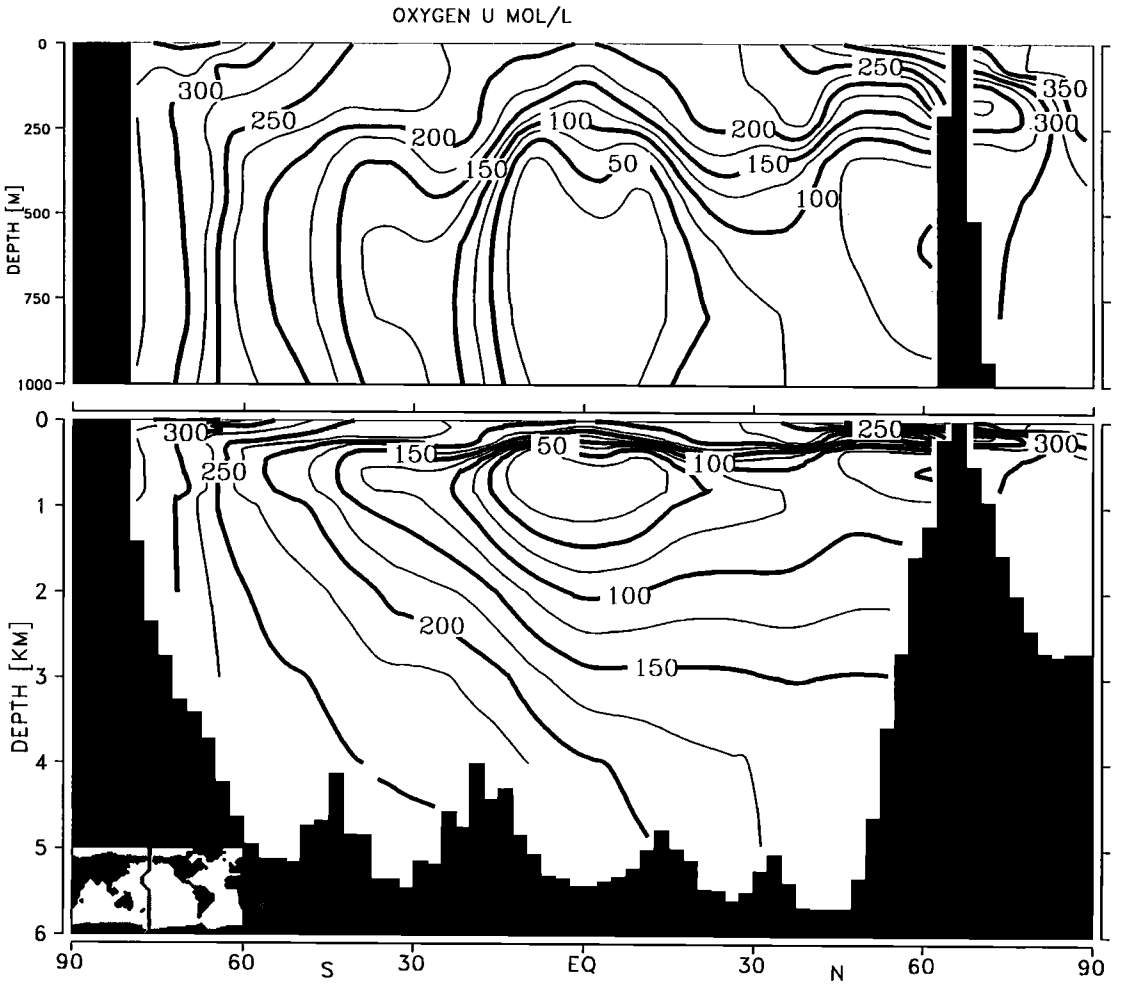


Fig. 4b. Oxygen along a section in the Western Pacific.

Redfield ratio of soft tissue. It provides an upper limit of 0.5 for the $C_{carb}/C_{org}$ rain ratio. The partitioning between carbonate and silicate producers is then

$$Pr\ Si = Psi\ (PSi\ /(PSi + PCO_3))$$

$$Pr\ CO_3 = PCO_3\ (PCO_3/(PCO_3 + PSi))$$

Silicate and carbonate are released to the interior ocean with an exponential penetration depth of 2 km for carbonate and 12 km for silicate. The choice of these numbers is rather arbitrary. For carbonate, at least, the assumption of a greater penetration depth than for soft tissue is supported by sediment trap data which show a general increase of the $C_{carb}/C_{org}$ ratio towards depth. During the formation of carbonate shells there is no fractionation between carbon isotopes [cf. Degens et al., 1984]. The high penetration depth of silicate yields a predominant silica dissolution near the bottom [cf. Broecker and Peng, 1983]. At locations where the silicious flux reaching the bottom exceeds 0.15 mol $m^{-2}$ $month^{-1}$, the excess is taken out from the system and interpreted as final deposition into sediment.

*Remineralization*

Provided there is enough oxygen we describe remineralization R with a temperature dependent rate:

$$R = (bo + b1(T+2))\ POC$$

where T is the temperature in centigrades, b1 =0.002/month/ °C, and bo is zero except in the bottom layer, where bo = 1/ 6 month

19449224, 1993, 3, Downloaded from https://agupubs.onlinelibrary.wiley.com/doi/10.1029/93GB01355 by MPI 348 Meteorology, Wiley Online Library on [11/01/2023]. See the Terms and Conditions (https://onlinelibrary.wiley.com/terms-and-conditions) on Wiley Online Library for rules of use; OA articles are governed by the applicable Creative Commons License

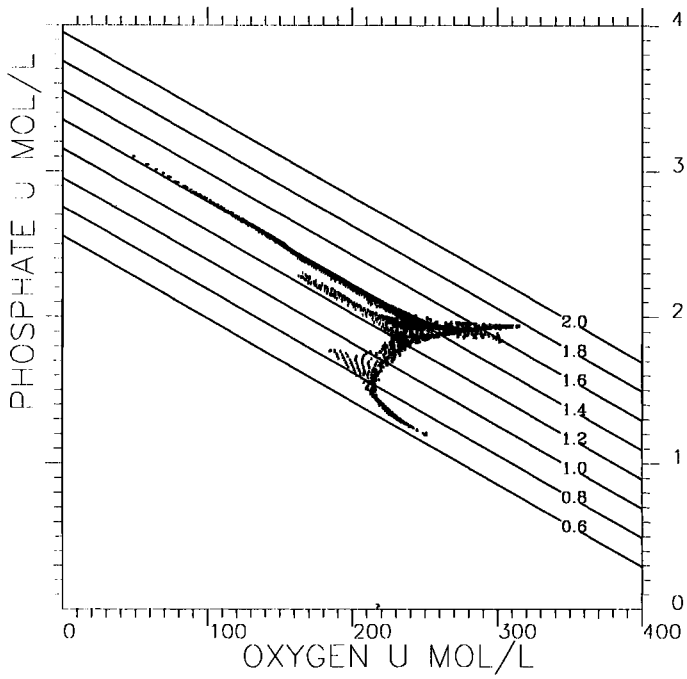


Fig. 5. Oxygen versus Phosphate in 3 km depth. The straight lines give the variation of PO4* = PO4 + O2/177 -1.95$\mu$ mol/l, according to the assumed Redfield ratio. The Atlantic deep water is at 0.7, the Weddell Sea water is at 1.8.

simulates the action of benthic organisms. During this process oxygen and alkalinity are reduced according to their respective Redfield ratios. The remineralized POC is added to the local concentrations of phosphate and $\Sigma CO_2$ in all three carbon isotopes.

At locations of oxygen deficit, the unremineralized POC is preserved and subject to advection. The resulting pool of POC reflects several shortcomings of the model: The equatorial upwelling is overestimated in the physical model and yields too high export production. In the real ocean, oxygen can be substituted by nitrate or sulfate which are not variables of the model. The distribution of POC in the model is thus an indication of where denitrification or sulfate reduction should occur when treated by the model.

During remineralization, the bacteria prefer the consumption of the light isotope $^{16}O_2$ [Craig and Kroopnick, 1970] with a fractionation of 0.982. The resulting isotope composition of dissolved oxygen in the water represents a rather unique tracer for a discrimination between circulation and remineralization effects in the oxygen distribution.

*Sediment Calcite-Carbonate System*

We take the dependency of the solubility product on salinity, temperature, and pressure from Broecker and Takahashi [1978] and compute locally the degree of saturation. We assume that calcite precipitation does not occur spontaneously, even in highly supersaturated water; the rate is too slow. Dissolution, in contrast, is assumed to work quickly. In the bottom layer, a small fraction ($10^{-5}$/month) of the sediment calcite is added to the calcite pool of the nearest-to-bottom layer where it is subject to dissolution. The undissolved fraction is put back to the sediment.

The sediment layer represents only the bioturbated upper 10 cm of the overall sediment. Sediment thickness is limited at 2 kmol $m^{-2}$ of carbon (i.e. 200 kg of $CaCO_3$); higher values are taken out. The resulting loss of carbon and alkalinity out of the system is in equilibrium with a compensating prescribed amount of river inflow along the coasts in the surface layer of 0.1 Gt/y carbon in the form of calcite with a zero content of $^{14}C$ and of $\delta^{13}C$. The model becomes stationary with a

19449224, 1993, 3, Downloaded from https://agupubs.onlinelibrary.wiley.com/doi/10.1029/93GB01355 by MPI 348 Meteorology, Wiley Online Library on [11/01/2023]. See the Terms and Conditions (https://onlinelibrary.wiley.com/terms-and-conditions) on Wiley Online Library for rules of use; OA articles are governed by the applicable Creative Commons License

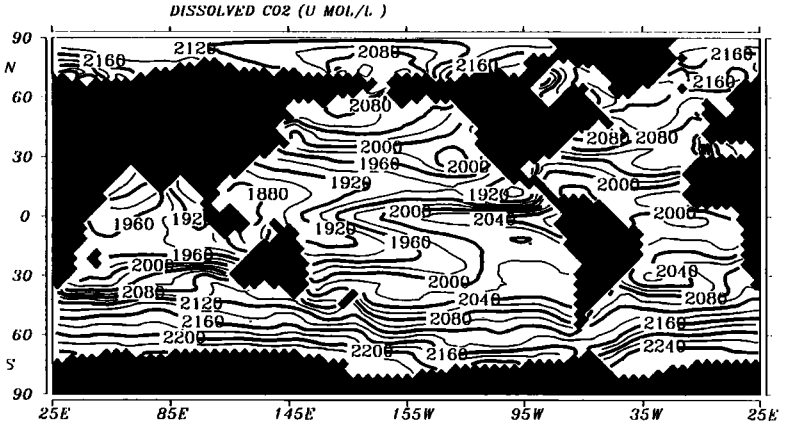


Fig. 6a. Annual mean dissolved inorganic carbon at the surface.

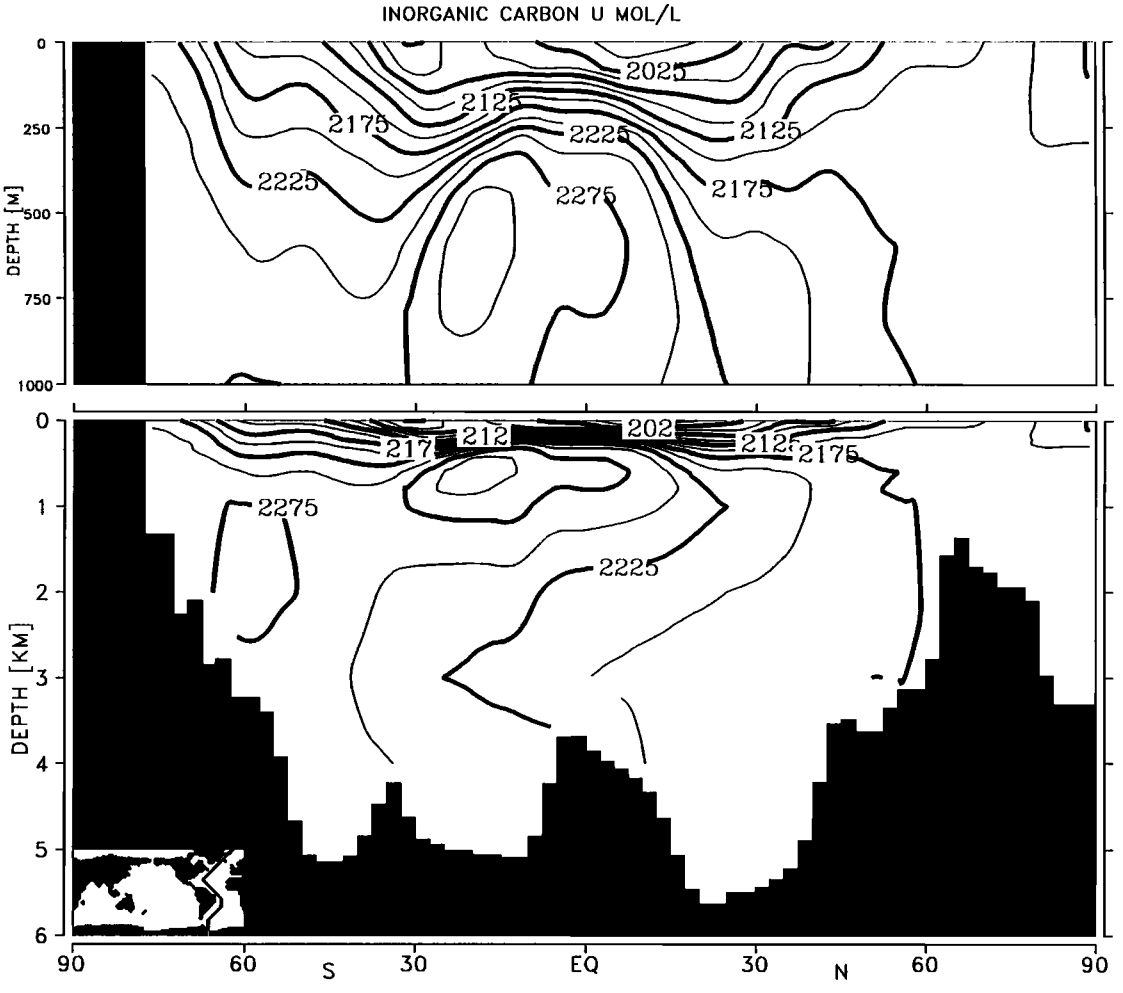


Fig. 6b. Dissolved inorganic carbon in the Western Atlantic.

19449224, 1993, 3, Downloaded from https://agupubs.onlinelibrary.wiley.com/doi/10.1029/93GB01355 by MPI 348 Meteorology, Wiley Online Library on [11/01/2023]. See the Terms and Conditions (https://onlinelibrary.wiley.com/terms-and-conditions) on Wiley Online Library for rules of use; OA articles are governed by the applicable Creative Commons License

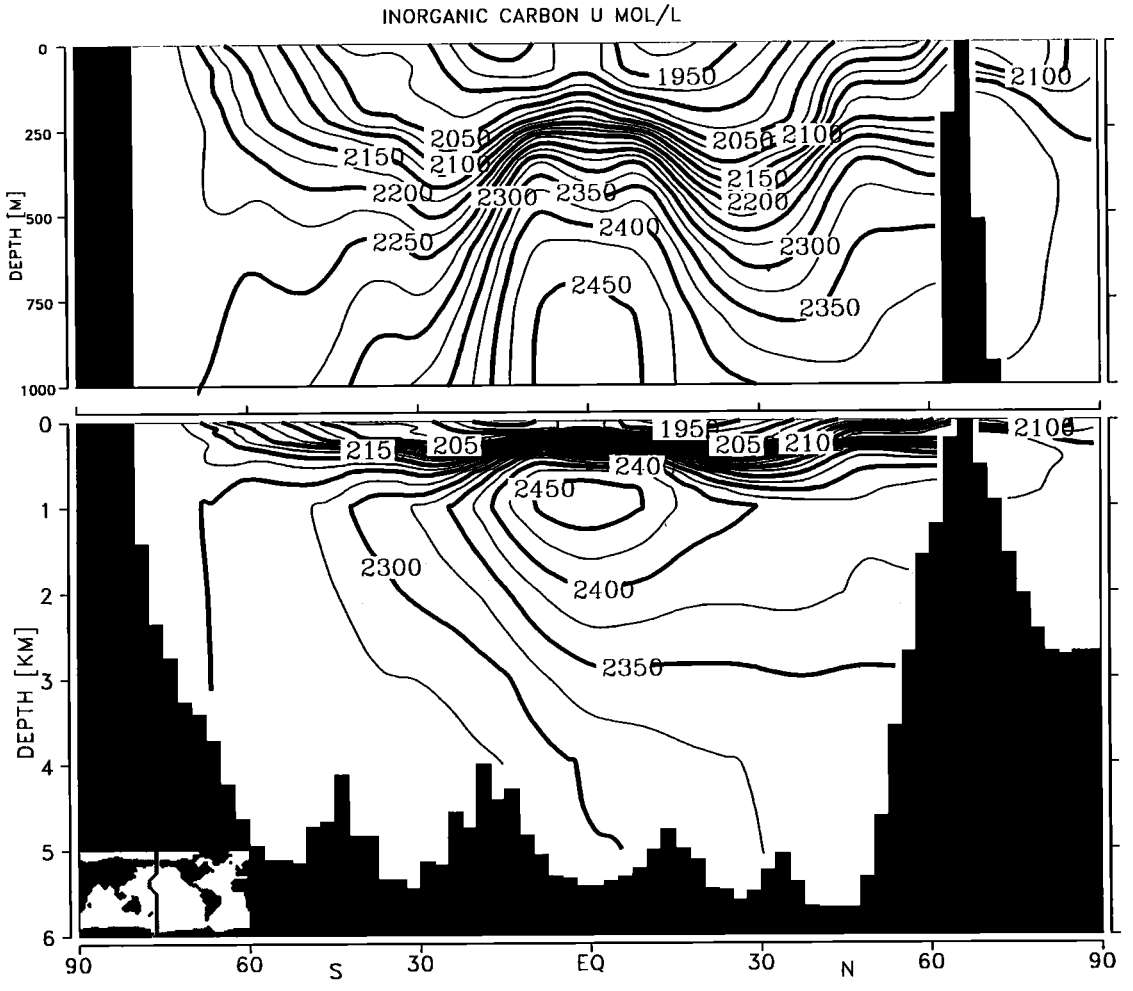


Fig. 6c. Dissolved inorganic carbon in the Western Pacific.

pool of 4500 Gt of carbon in the form of calcite. The global average time constant of the sediment system is thus on the order of 45000 years. Locally, the time constant varies with the degree of supersaturation of the surrounding water; it may reduce substantially in an environment of increasing $CO_2$.

No fractionation is assumed in these dissolution processes. The sediment and calcite pools are treated nevertheless for all three isotopes for an exact budgeting of the individual types of atoms since the particulate matter is formed at the sea surface in environments of varying isotopic compositions.

## 3. THE STATIONARY (PREINDUSTRIAL) STATE

### *The Nutrient-Oxygen Cycle*

The surface distribution of the variables is mainly determined by the structure of the surface temperature, which results from the prescribed atmospheric temperature, and by the vertical component of water flow, which reflects primarily the input of vorticity by the prescribed windfield. Figure 1b shows the annual mean vertical velocity at the base of the uppermost model layer (at 50 m). The dominant features are the strong equatorial upwelling in Atlantic and Pacific, moderate upwelling along the western coasts and in the Antarctic Circumpolar Current (ACC), and downwelling in the subtropical gyres. Many regional structures like the West African coastal upwelling cannot be resolved in such a coarse model.

The supply of nutrients by upwelling feeds the biological pump which acts directly as the main cause for the tracer distributions as discussed below. Figure 1c displays the annual mean production of soft tissue. The structure is dominated by the

19449224, 1993, 3, Downloaded from https://agupubs.onlinelibrary.wiley.com/doi/10.1029/93GB01355 by MPI 348 Meteorology, Wiley Online Library on [11/01/2023]. See the Terms and Conditions (https://onlinelibrary.wiley.com/terms-and-conditions) on Wiley Online Library for rules of use; OA articles are governed by the applicable Creative Commons License

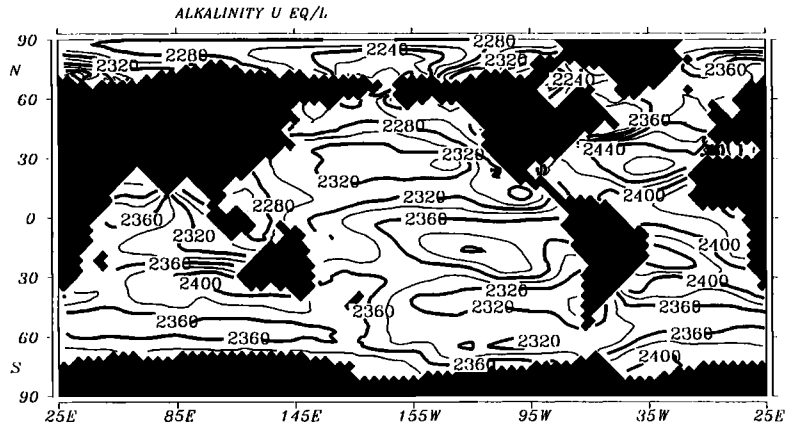


Fig. 7a. Annual mean surface alkalinity.

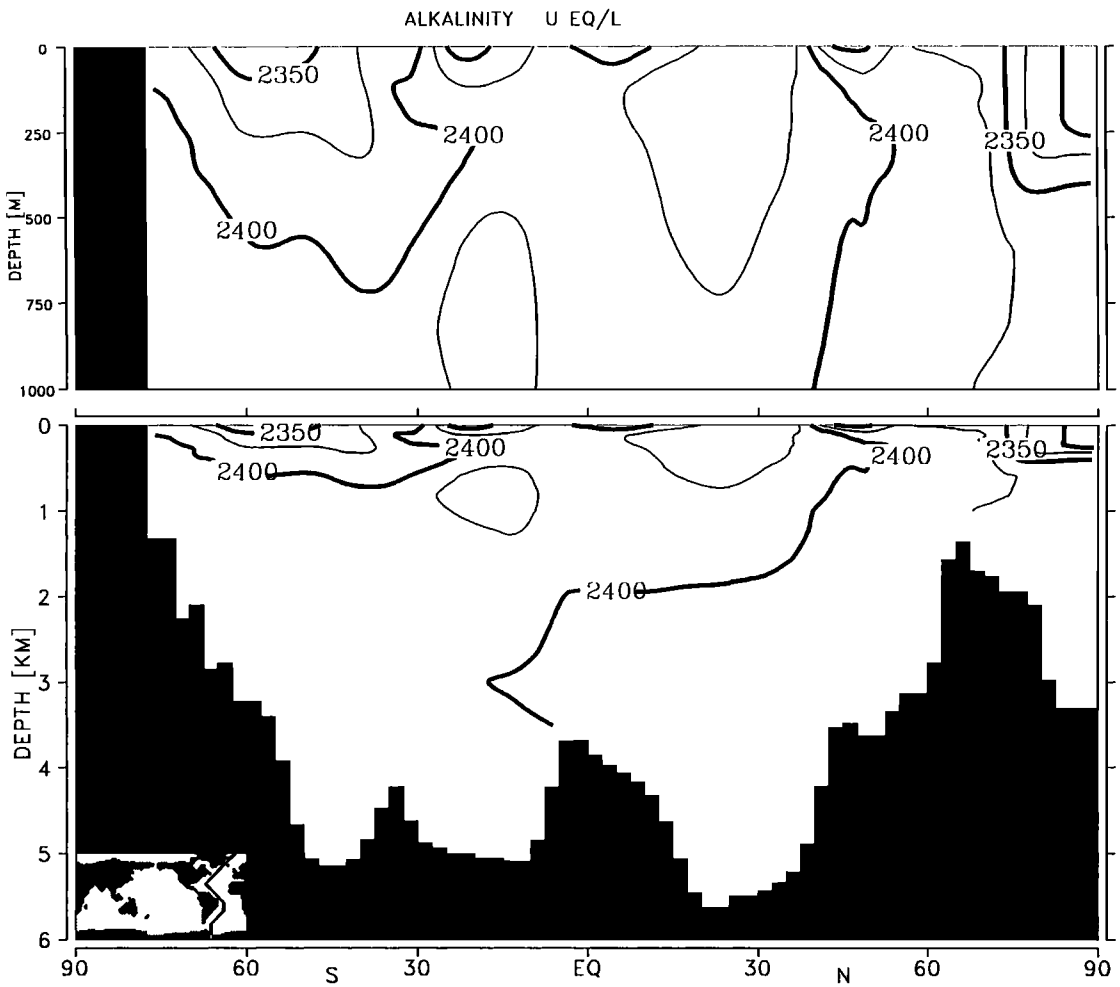


Fig. 7b. Alkalinity in the Western Atlantic.

19449224, 1993, 3, Downloaded from https://agupubs.onlinelibrary.wiley.com/doi/10.1029/93GB01355 by MPI 348 Meteorology, Wiley Online Library on [11/01/2023]. See the Terms and Conditions (https://onlinelibrary.wiley.com/terms-and-conditions) on Wiley Online Library for rules of use; OA articles are governed by the applicable Creative Commons License

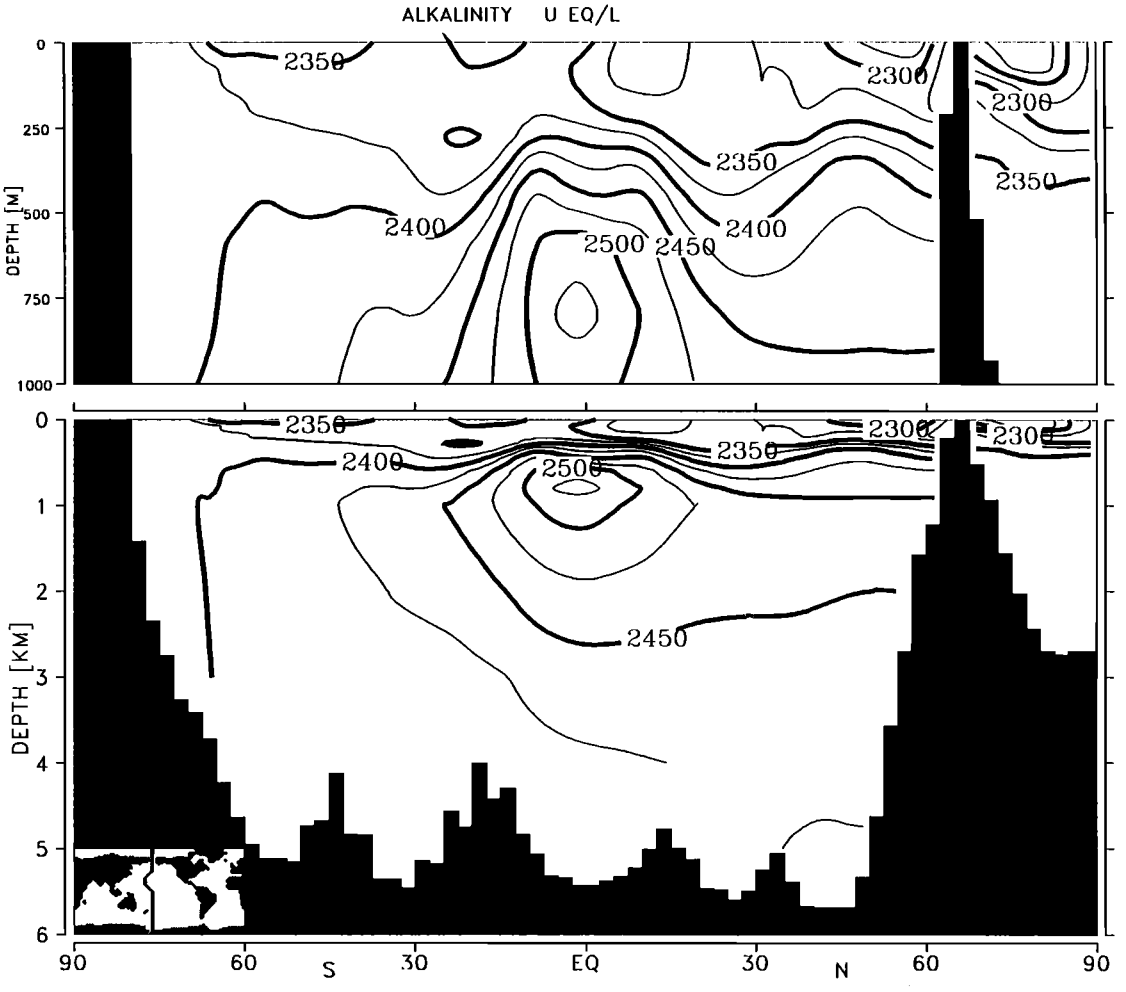


Fig. 7c. Alkalinity in the Western Pacific.

upwelling. Since the model allows for maximally 25 % of the local phosphate concentration to be removed per time step, the structures are smoother than those of the upwelling. In the subtropical gyres with predominant downwelling, the production is only a few percent of the (perhaps overestimated) equatorial maximum. In high latitudes, the production is limited by the physical conditions rather than by nutrient deficits. The production of hard parts is displayed in terms of rain ratios: Figure 1d shows the $C_{carb}:C_{org}$ ratio. The maxima are in the subtropical gyres, where temperature and the absence of silicate favor the production of calcite shells. The minimum at the equator is caused by the strong upwelling of silicate which is incorporated preferentially. Towards higher latitudes the ratio also diminishes according the assumed temperature dependency of calcite production. These mechanisms are also seen in the distribution of opal to calcite ratio (Figure 1e). The peculiar maximum towards the coast, especially near Southern America, is merely an artefact of the model configuration: The loss of silicate into the sediment is compensated by a homogeneous river input of silicate along all coasts (except Antarctica). The almost perfect geostrophic balance in the circulation field inhibits the ventilation of semienclosed near-to-coast grid points at meridional coast lines.

The structure of the upwelling is seen also in the distributions of surface phosphate (Figure 2a) and surface silicate

19449224, 1993, 3, Downloaded from https://agupubs.onlinelibrary.wiley.com/doi/10.1029/93GB01355 by MPI 348 Meteorology, Wiley Online Library on [11/01/2023]. See the Terms and Conditions (https://onlinelibrary.wiley.com/terms-and-conditions) on Wiley Online Library for rules of use; OA articles are governed by the applicable Creative Commons License

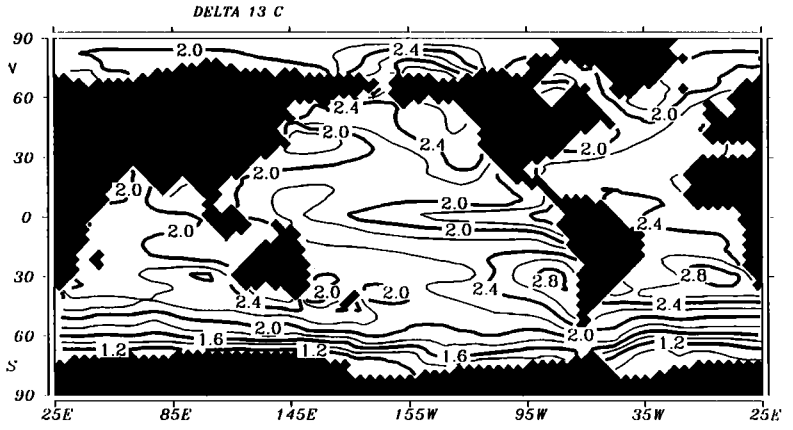


Fig. 8a. Distribution of $\delta^{13}C$ at sea surface.

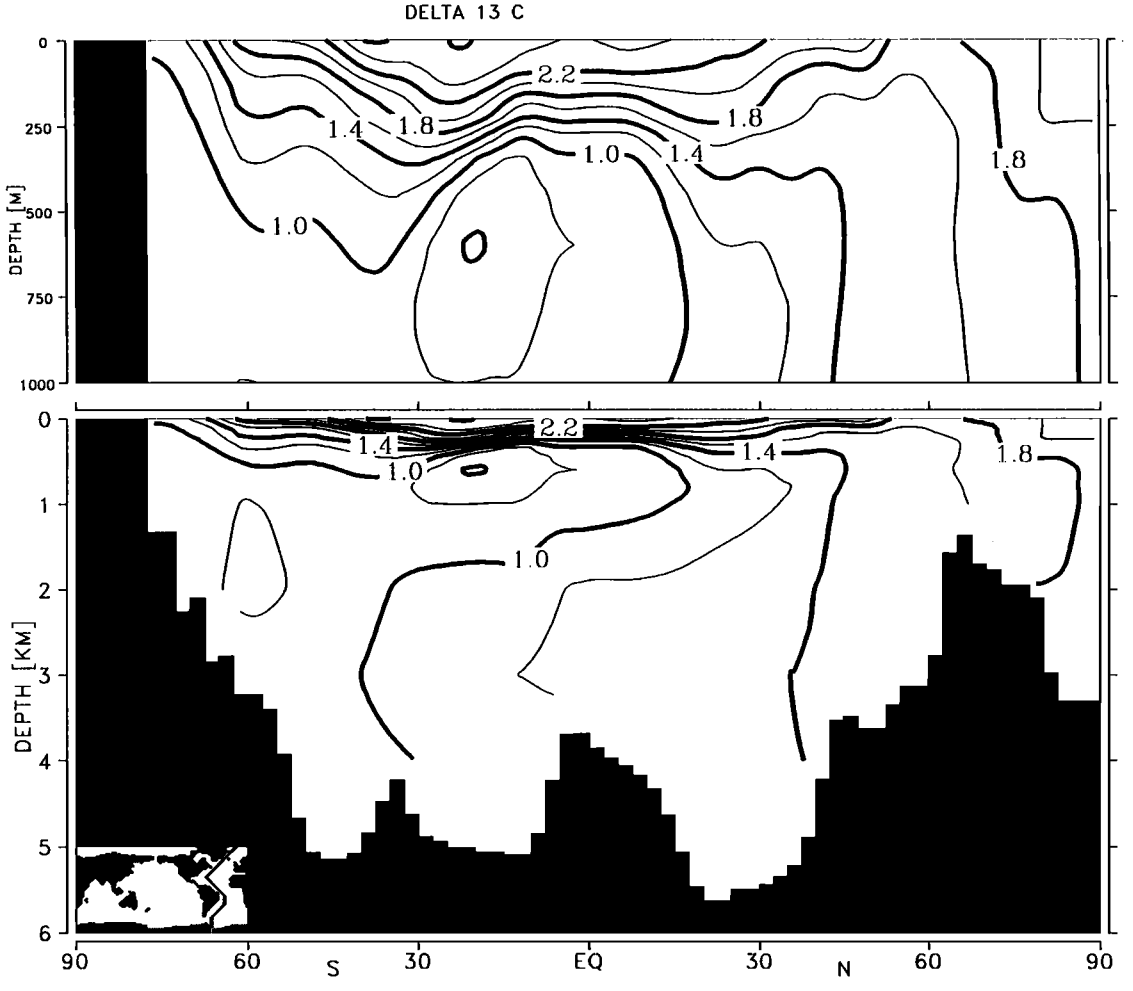


Fig. 8b. Distrinution of $\delta^{13}C$ in the Western Atlantic.

19449224, 1993, 3, Downloaded from https://agupubs.onlinelibrary.wiley.com/doi/10.1029/93GB01355 by MPI 348 Meteorology, Wiley Online Library on [11/01/2023]. See the Terms and Conditions (https://onlinelibrary.wiley.com/terms-and-conditions) on Wiley Online Library for rules of use; OA articles are governed by the applicable Creative Commons License

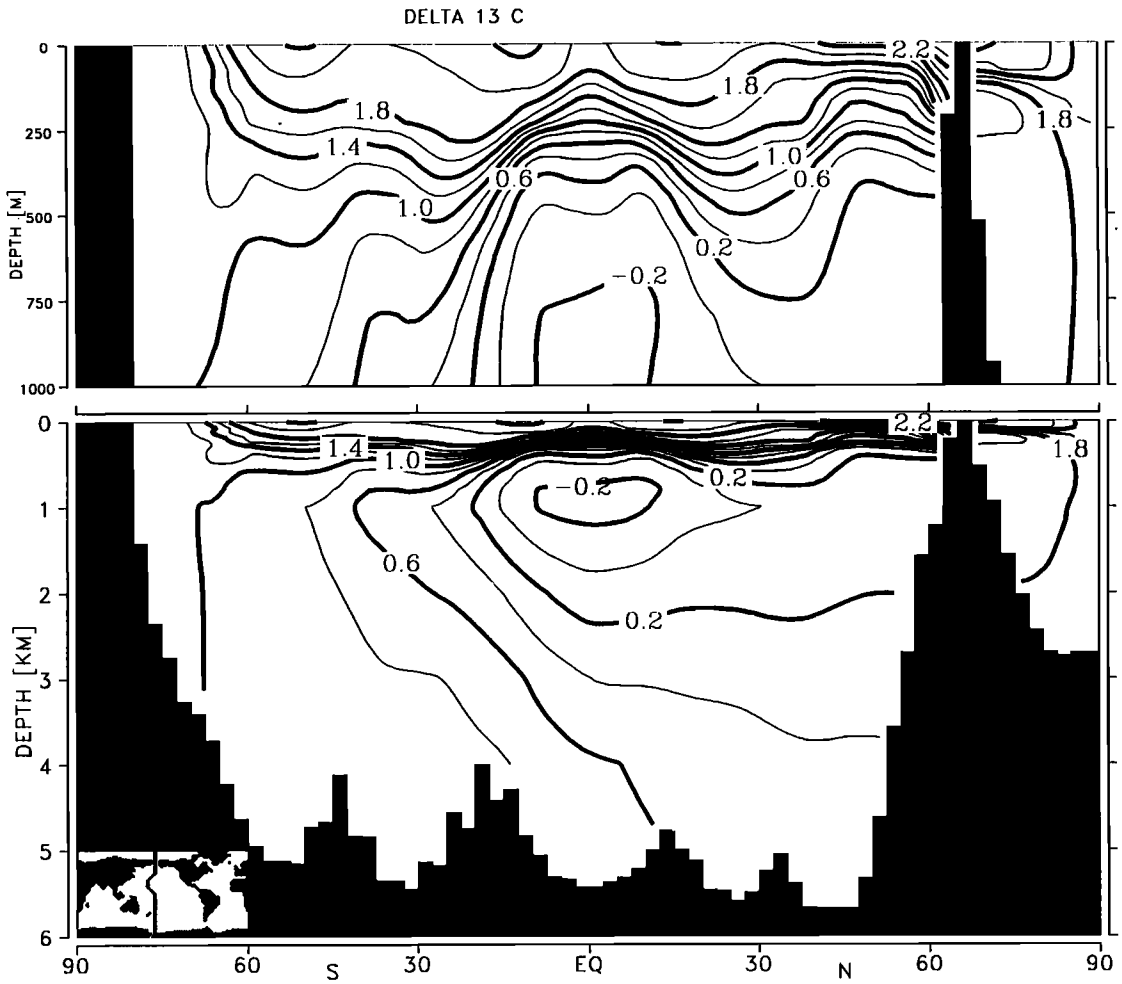


Fig. 8c. Distribution of $\delta^{13}C$ in the Western Pacific.

(Figure 2b). Distinct differences in the patterns are in high latitudes. Here, obviously, the productivity is not limited by nutrients; the reduction of the productivity, as derived from observations, too, [Koblents - Mishke, 1977], may be caused by ice cover and weaker insolation as well as by high turbulence [cf. Radach and Maier-Reimer, 1975]. The deep distributions of phosphate and silicate (Figures 3a, 3b, 3c, and 3d) both reflect the conveyor belt structure of Figure 1a. The circulation supports a depletion in the Northern Atlantic and an enrichment in the Northern Pacific. The gradients of silicate are much stronger than those of phosphate due to the assumption of stronger surface depletion and deeper penetration for silicate.

The distribution of dissolved oxygen (figs. 4a and 4b) has partly similar structure to the phosphate distributions, especially in the deep Pacific, where the phosphate maximum is found in almost anoxic water. The Atlantic is generally higher in oxygen, corresponding to the lower phosphate content which overrules the lower solubility due to the higher temperature. The correlation between oxygen and phosphate is shown in Figure 5. In the Indian and in the Pacific ocean most of the values are on the line defined by the assumed constant Redfield ratio. In the Atlantic, however, the scatter diagram is dominated by the mixing between the two end members of NADW and WSBW. The Redfield combination PO4* = PO4 + O2/177 - 1.95 defines a quantity in which the effects of

19449224, 1993, 3, Downloaded from https://agupubs.onlinelibrary.wiley.com/doi/10.1029/93GB01355 by MPI 348 Meteorology, Wiley Online Library on [11/01/2023]. See the Terms and Conditions (https://onlinelibrary.wiley.com/terms-and-conditions) on Wiley Online Library for rules of use; OA articles are governed by the applicable Creative Commons License

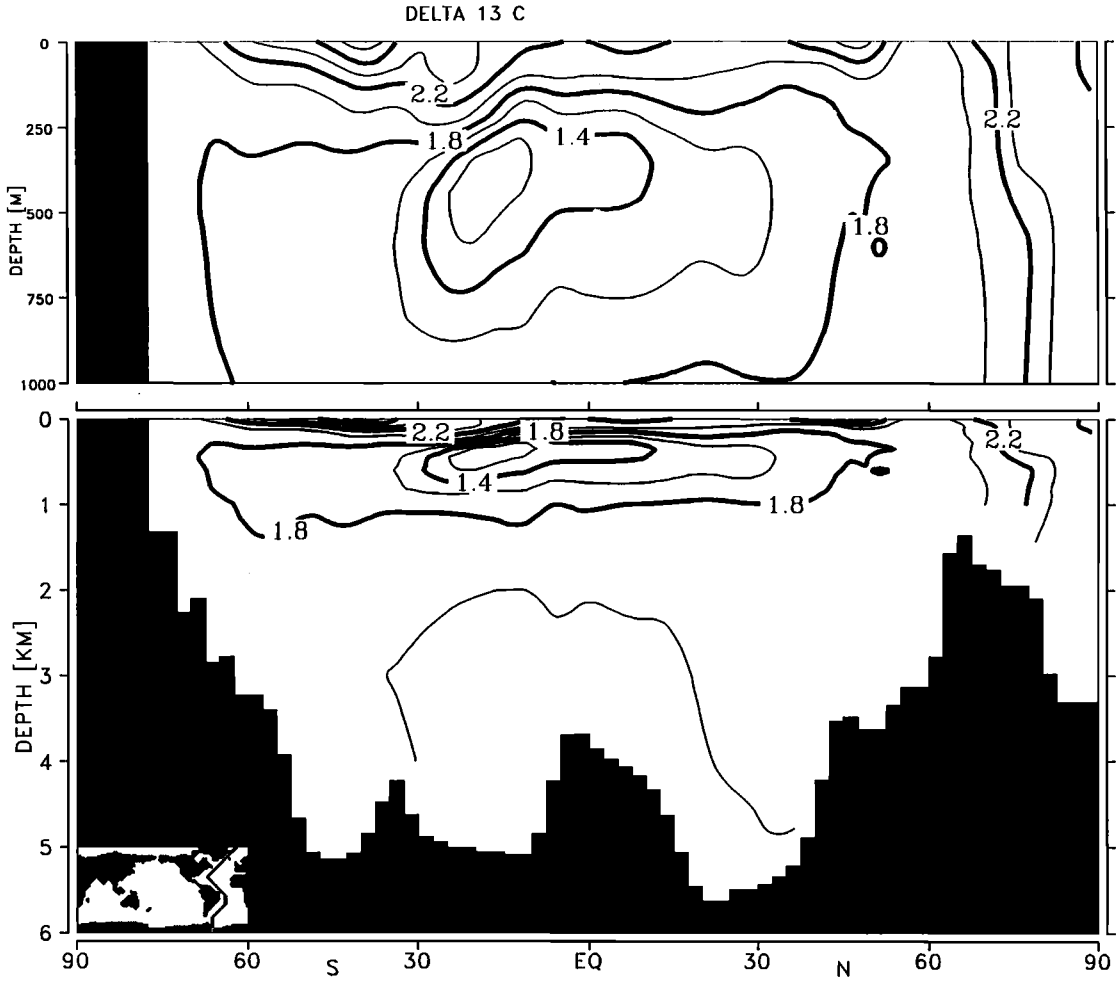


Fig. 8d. Distribution of $\delta^{13}C$ with fractionation according Rau et al [1991].

the details of the remineralization are cancelled out. It can be regarded as a physical tracer [Broecker et al., 1991]. The value 1.95 is arbitrarily subtracted in order to obtain similar numbers as for phosphate. The distribution is dominated by mixing effects between the endmembers NADW at 0.7 and WSBW at 1.8. In the northern and central Pacific the distribution is almost uniform at values between 1.35 and 1.4, which indicates a mixing ratio of 30:70 between NADW and WSBW.

### *Dissolved CO2 and Alkalinity*

The global inventories of the tracers are not precisely enough known to be used as initialization, even if the model would be perfect. Due to lon adjustment time of the sediment pool, no systematic tuning to all observational constraints was possible. The preindustrial $pCO_2$ of 280 ppm in the atmosphere was considered to be the most important criterion for the settings. After a preliminary global uniform setting with typical numbers for the deep southern ocean, the alkalinity inventory was tuned to produce an atmospheric partial pressure of 280 ppm with the given carbon pool. The surface distribution of $\Sigma CO_2$ is dominated by the SST (Figure 6a), whereas the surface alkalinty (Figure 7a) reflects rather the structure of surface salinity. Figures 6b, 6c, 7b, and 7c show the sections for both variables. Since the net effect of temperature on the concentration of $\Sigma CO_2$ accounts for only 70 μmol/L [Maier-Reimer and Hasselmann, 1987], the gradients in the distributions are maintained primarily by the biological processes. In the global average, the model exhibits a rain ratio of calcium carbonate

19449224, 1993, 3, Downloaded from https://agupubs.onlinelibrary.wiley.com/doi/10.1029/93GB01355 by MPI 348 Meteorology, Wiley Online Library on [11/01/2023]. See the Terms and Conditions (https://onlinelibrary.wiley.com/terms-and-conditions) on Wiley Online Library for rules of use; OA articles are governed by the applicable Creative Commons License

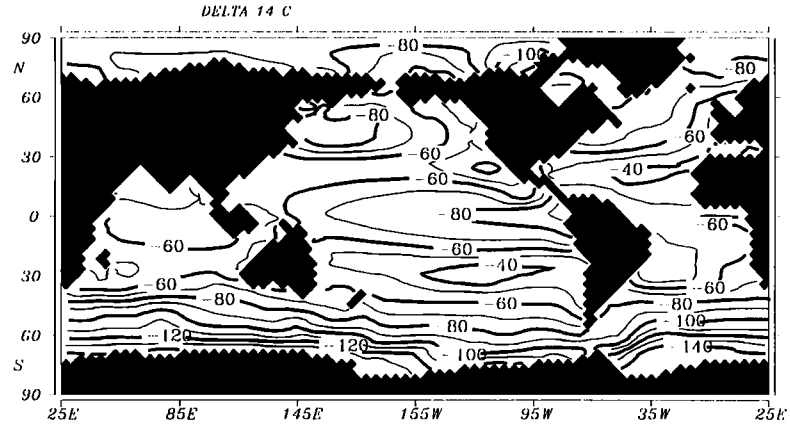


Fig. 9a. Distribution of $\Delta^{14}C$ (preindustrial) at sea surface.

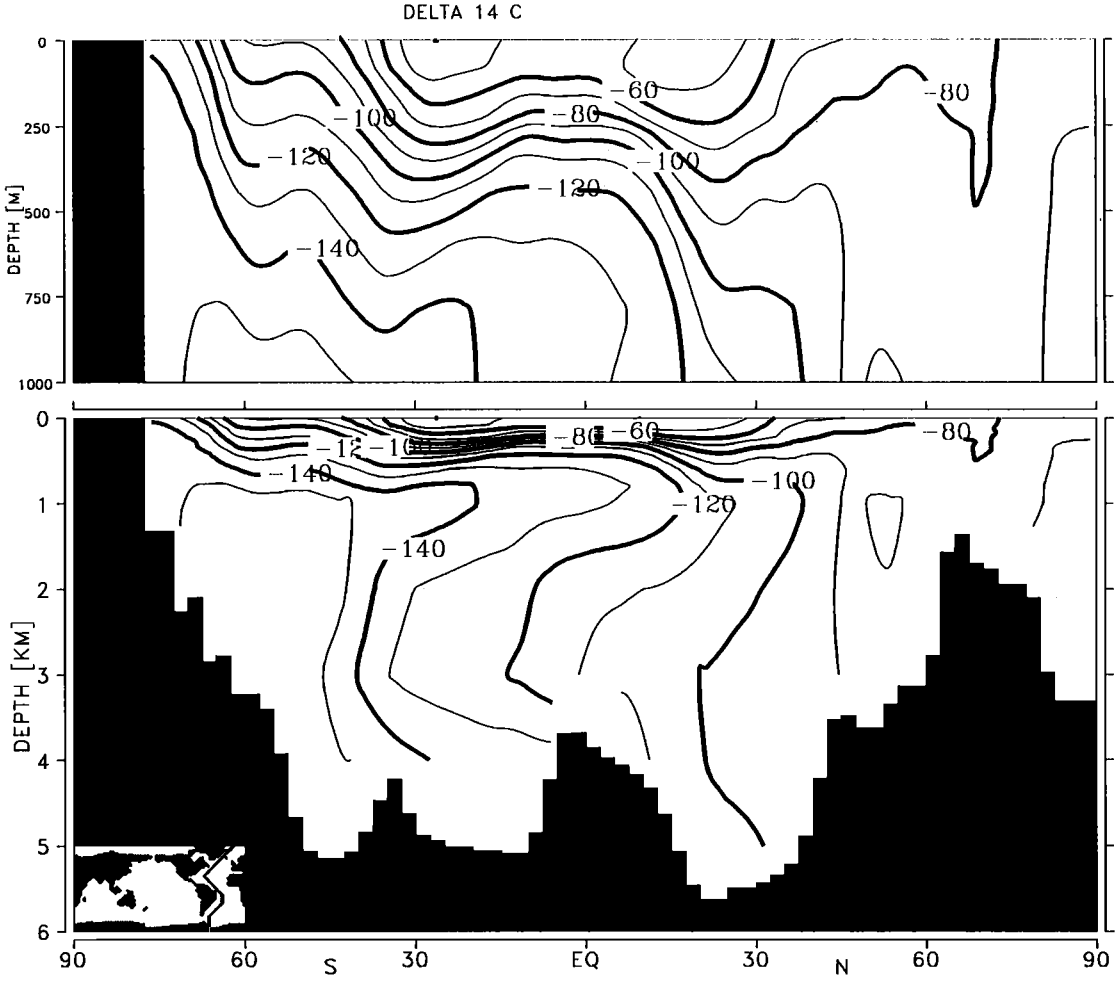


Fig. 9b. Distribution of $\Delta^{14}C$ (preindustrial) in the Western Atlantic.

19449224, 1993, 3, Downloaded from https://agupubs.onlinelibrary.wiley.com/doi/10.1029/93GB01355 by MPI 348 Meteorology, Wiley Online Library on [11/01/2023]. See the Terms and Conditions (https://onlinelibrary.wiley.com/terms-and-conditions) on Wiley Online Library for rules of use; OA articles are governed by the applicable Creative Commons License

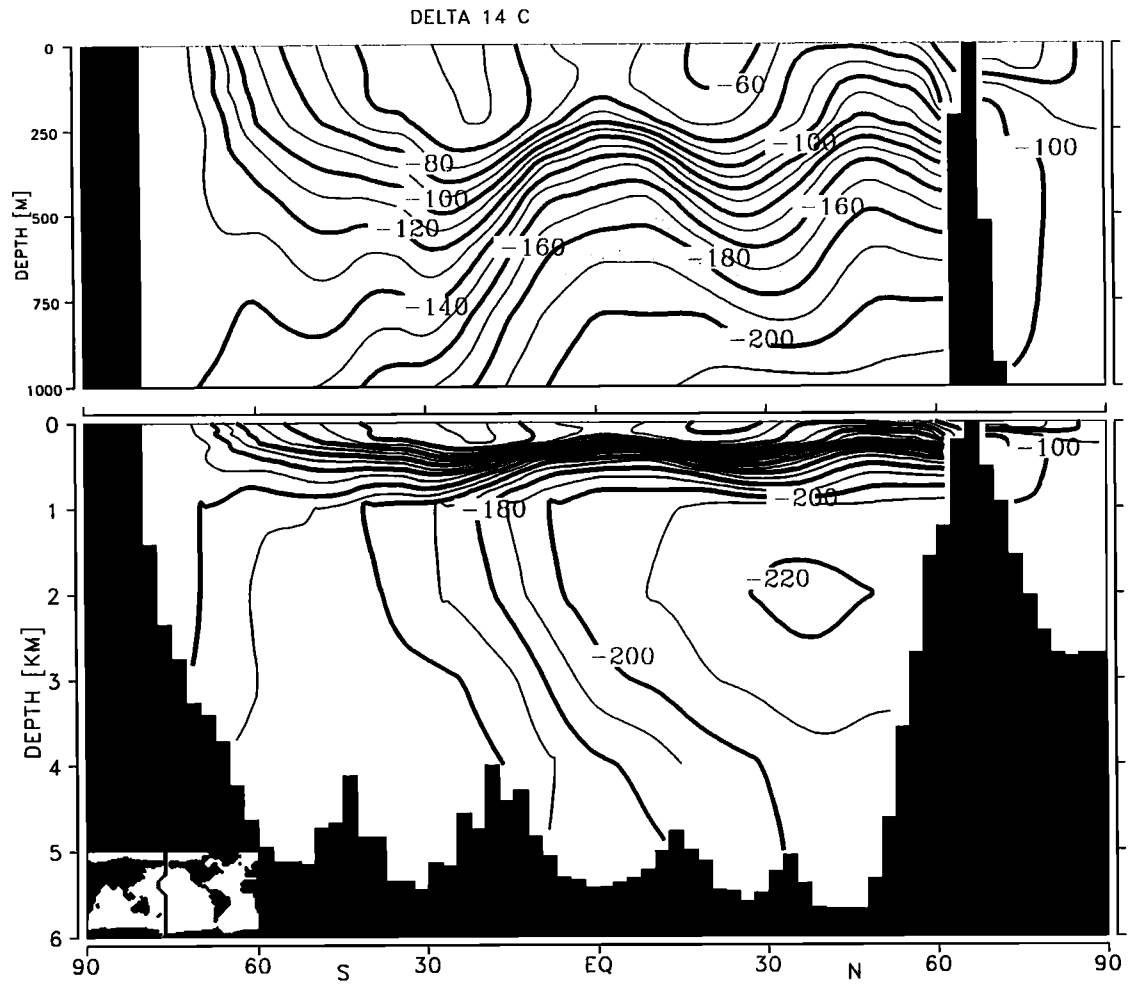


Fig. 9c. Distribution of $\Delta^{14}C$ (preindustrial) in the Western Pacific.

to organic material of 0.22. This relation in the productivity makes the gradients of $\Sigma CO_2$ about 4 times bigger than the gradients of alkalinity. Both distributions again reflect the conveyor belt structure with a relative depletion of Atlantic waters as compared to the Pacific.

*Carbon Isotopes*

The surface map of $\delta^{13}C$ (Figure 8a) is dominated by the opposing effects of temperature and productivity on the the fractionation of isotopes: in the equatorial belt of high productivity, the temperature tends to deplete the $^{13}C$ content, whereas the formation of soft tissue enrichens the water in $^{13}C$. On a global scale, the gradient is dominated by the productivity, but halved by temperature. The sections of $\delta^{13}C$ are shown in Figures 8b and 8c. The global pattern agrees with Kroopnick's [1985] representation for the deep ocean, where no Suess effect exists. The constant offset of approximately half per mill is caused by the numerical values of the thermodynamic fractionation coefficients.

Newer results [Rau et al., 1991] indicate that the fractionation effect depends on the local concentration of dissolved gaseous $CO_2$, i.e., strongly on temperature. They propose a functional relationship:

$$Fp^{13} = 1+0.001(((3.4-17\ \log(Caq))/1000+1)$$

$$(996.1-0.3\ Caq)-999),$$

and $Fp^{14} = (Fp^{13})^2$, where $Caq$ denotes the concentration of gaseous $CO_2$.

19449224, 1993, 3, Downloaded from https://agupubs.onlinelibrary.wiley.com/doi/10.1029/93GB01355 by MPI 348 Meteorology, Wiley Online Library on [11/01/2023]. See the Terms and Conditions (https://onlinelibrary.wiley.com/terms-and-conditions) on Wiley Online Library for rules of use; OA articles are governed by the applicable Creative Commons License

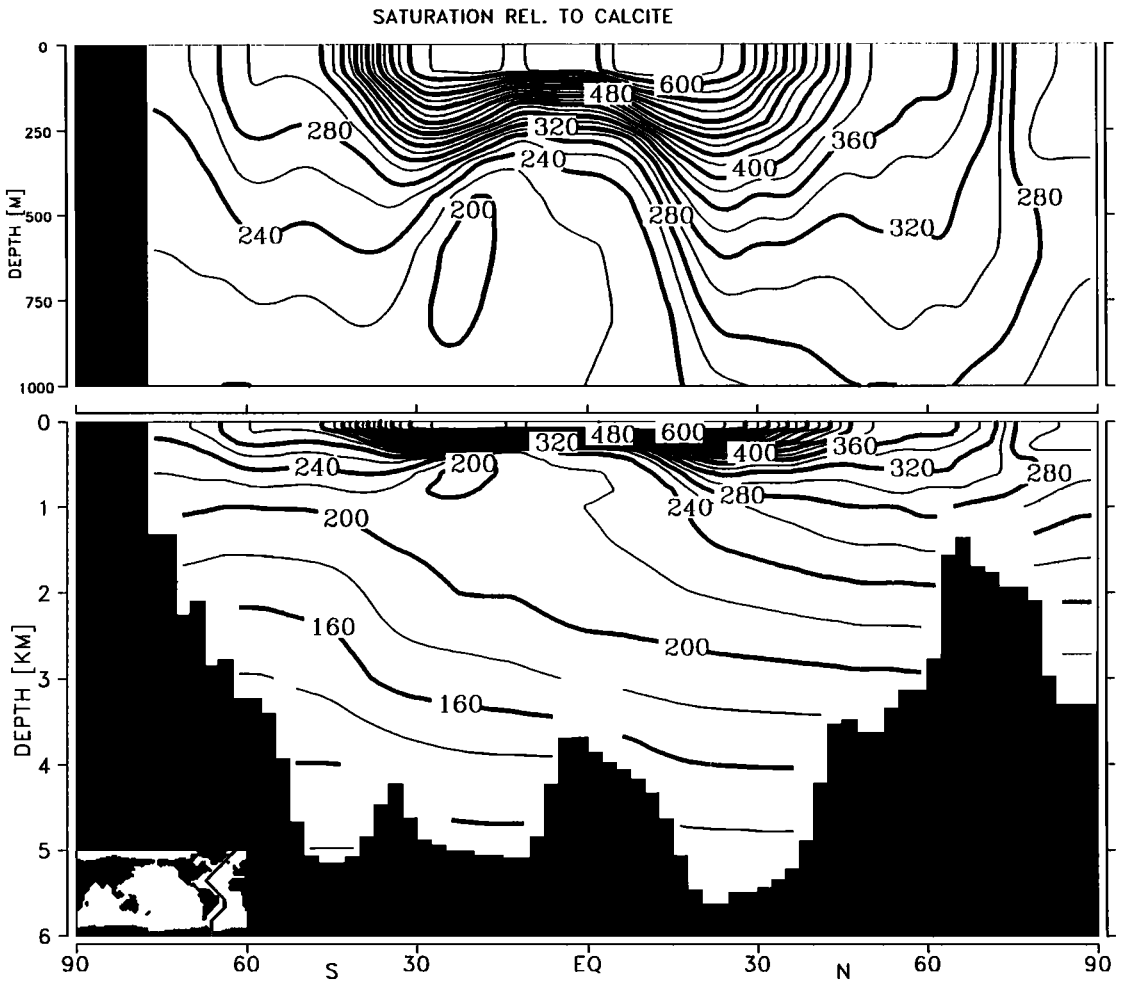


Fig. 10a. Degree of saturation with respect to calcite in the Western Atlantic.

The model was run with this formulation, too. Figure 8d shows the resulting section for $\delta^{13}C$ in the Western Atlantic. The main difference to Figure 8b is the lack of structure of Antarctic intermediate water. Obviously, this formulation creates too much violation of the observed correlation between phosphate and $\delta^{13}C$.

The surface distribution of $\Delta^{14}C$ (Figure 9a) is dominated by the effective connection with deeper waters. In the subtropical gyres, the $^{14}C$ content is almost in equilibrium with the atmosphere; in upwelling regions, the equilibration with the atmosphere is modified by the variations of the gas exchange. The extreme low in the eastern Pacific in the region of strong upwelling is probably overestimated. Figures 9b and 9c display the simulated preindustrial sections of $\Delta^{14}C$ along the GEOSECS sections. The Atlantic appears to be slightly too old, whereas the Pacific is slightly too young. The latter flaw is almost homogeneous in the whole Pacific.

Obviously, the model produces too much mixing in the circum-Antarctic part of the Pacific. The deep water starts with a value of - 140 instead of - 160 as in the real ocean.

*Carbonates*

Figures 10a and 10b show sections of the degree of supersaturation with respect to calcite. Here again, the conveyor belt structure of the circulation yields significant differences between the oceans. The lack of phosphate in the Atlantic yields a lower productivity (less

19449224, 1993, 3, Downloaded from https://agupubs.onlinelibrary.wiley.com/doi/10.1029/93GB01355 by MPI 348 Meteorology, Wiley Online Library on [11/01/2023]. See the Terms and Conditions (https://onlinelibrary.wiley.com/terms-and-conditions) on Wiley Online Library for rules of use; OA articles are governed by the applicable Creative Commons License

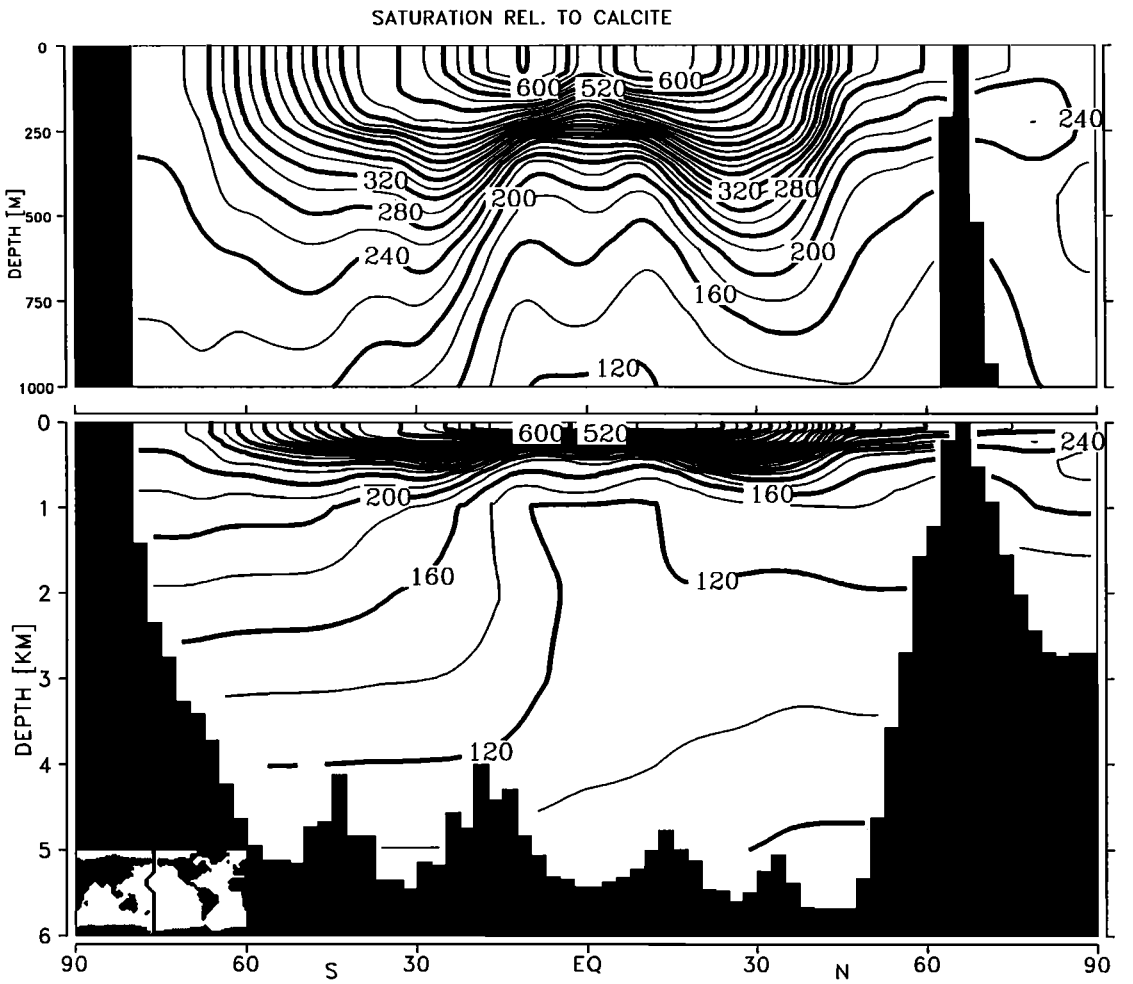


Fig. 10b. Degree of saturation with respect to calcite in the Western Pacific.

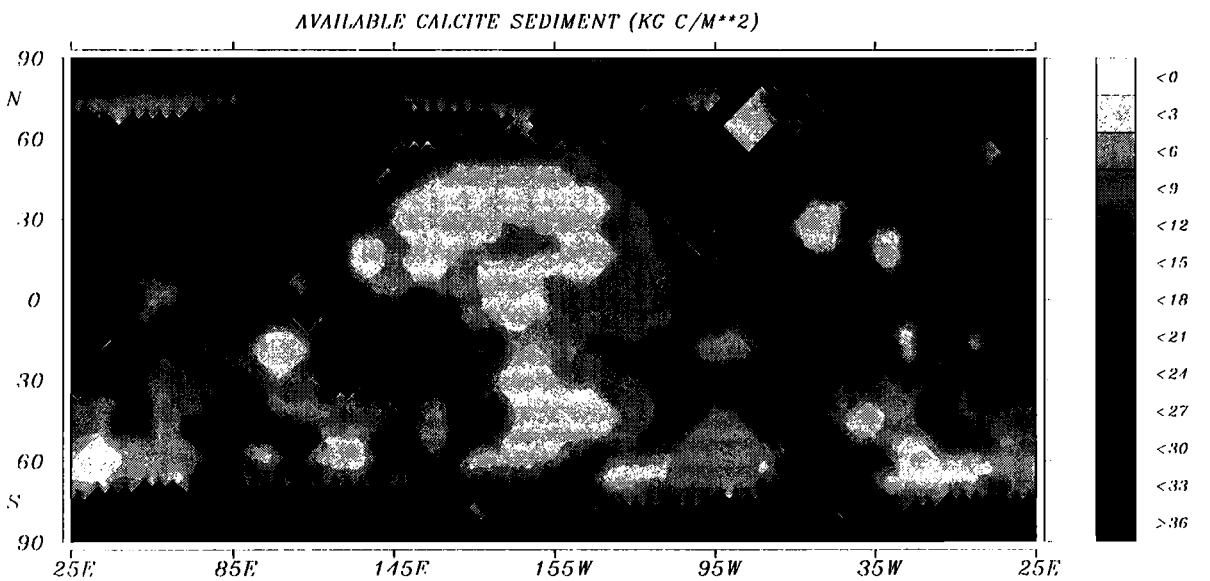


Fig. 10c. Bioturbated calcite in the sediment.

19449224, 1993, 3, Downloaded from https://agupubs.onlinelibrary.wiley.com/doi/10.1029/93GB01355 by MPI 348 Meteorology, Wiley Online Library on [11/01/2023]. See the Terms and Conditions (https://onlinelibrary.wiley.com/terms-and-conditions) on Wiley Online Library for rules of use; OA articles are governed by the applicable Creative Commons License

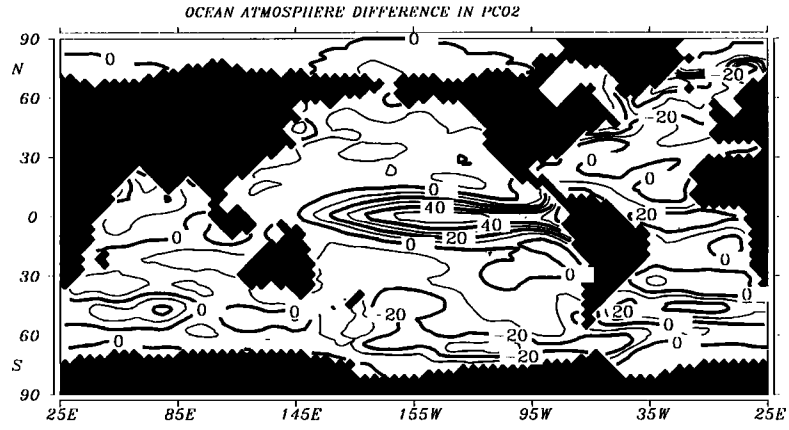


Fig. 11. Annual mean sea-air difference in $CO_2$ partial pressure.

alkalinity consumption during remineralization) which is due to the strong lack of silicate shifted to a higher rain ratio of $CaCO_3$ (relatively more alkalinity release by calcite dissolution). Both mechanisms tend to shift the lysocline to deeper horizons. Figure 10c shows the thickness of the sediment of calcium carbonate resulting from the rain exerted by the export productivity and the intersection of the lysocline with the topography. The basic structure is given by the 3-km isobath in the Pacific. In the Atlantic, where the lysocline level is deeper, the sediment covers a larger percentage of the ocean floor.

*Surface Partial Pressure of* $CO_2$

The model's annual mean $CO_2$ difference between sea surface and atmosphere (Figure 11) shows a strong high in the equatorial Pacific, a high in the equatorial Atlantic off the coast of Africa, and lows at high latitudes. As a consequence of the assumed constant gas exchange coefficient the strength of the equatorial high is underestimated. Lower values are seen in the western Pacific and western Atlantic than further east, as the gyre surface flow carries warm water northward where it rapidly cools. These structures are all seen in data of $CO_2$ in surface ocean water [Keeling, 1968; Takahashi et al., 1983], which, additionally, reflect the changes of the air-sea difference of $pCO_2$ by the increased $CO_2$ content of the atmosphere in the last century [Maier-Reimer and Hasselmann, 1987]. The distribution of $PCO_2$ shows a pronounced seasonality resulting from a delicate balance of physical and biological effects. In spring, the biological pump begins to act with the onset of the plankton bloom at reduced turbulence and increased temperature. In some regions of the subpolar oceans, the seasonality is inverse to the temperature effect.

*Isotopes of dissolved* $O_2$

During bacterial remineralization of organic matter, the consumption of the light isotop $^{16}O$ is preferred with a fractionation of 18 permille [Schlesser, 1979]. Craig and Kroopnik [1970] have pointed out, that the resulting isotopic ratio $\delta^{18}O$ of dissolved oxygen in sea water is the only bioactive tracer which systematically varies nonlinearly with the others and may, thus, serve as a constraint to decouple the effects of circulation and respiration on the distribution of dissolved oxygen. Bender [1990] has compared existing measurements with four extremely simplified models of ocean circulation. In these comparisons, he found that fractionation factor $\alpha=0.982$ is probably too small to be representative for the entire ocean. In the absence of mixing, the isotopic ratio would follow the law:

$$\delta^{18}O = 1000\ (\alpha-1)\ \ln([O_2]/[O_2]_{sat})$$

In contrast to this formula, the observed $\delta^{18}O$ does not exceed 20 permille. The deductions from these simplified models are confirmed by the results of our model: Figure 12 shows the covariation between $\delta^{18}O$ and relative oxygen saturation in the depth horizons below 500 m together with the corresponding scatter of the GEOSECS data [Kroopnick, 1987]. For oxygen

19449224, 1993, 3, Downloaded from https://agupubs.onlinelibrary.wiley.com/doi/10.1029/93GB01355 by MPI 348 Meteorology, Wiley Online Library on [11/01/2023]. See the Terms and Conditions (https://onlinelibrary.wiley.com/terms-and-conditions) on Wiley Online Library for rules of use; OA articles are governed by the applicable Creative Commons License

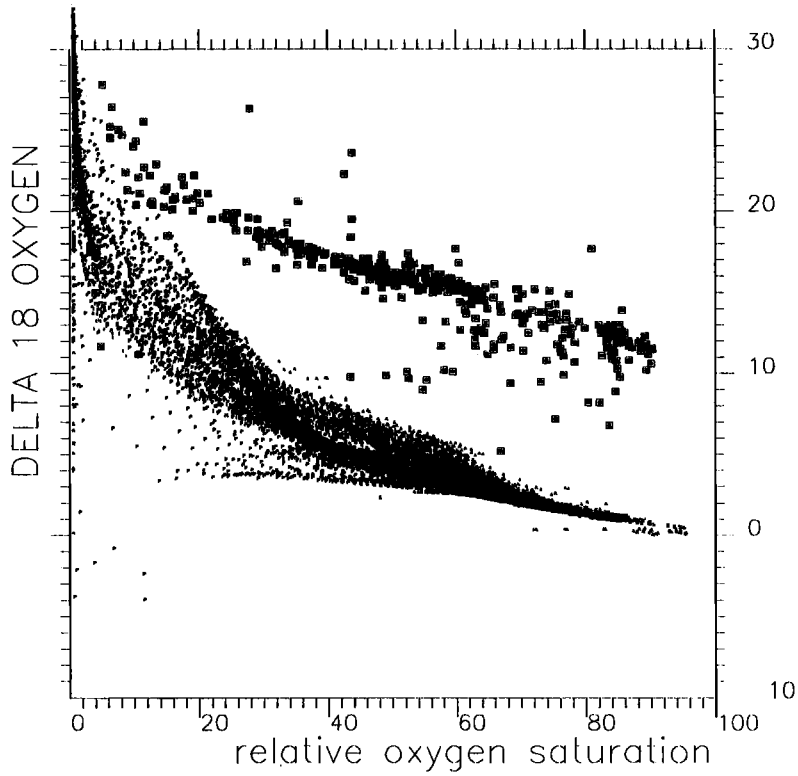


Fig. 12. Scatter of $\delta^{18}O$ versus relative oxygen saturation below 500 m. The open squares display all GEOSECS data [Kroopnick, 1987], shifted by 10 permille for $\delta^{18}O$.

concentrations higher than 30% of the temperature dependent saturation value, the dots follow closely the slope of observations, corresponding the slope determined by the fractionation. For higher degrees of oxygen utilization, the models distribution of $\delta^{18}O$ starts to become sytematically too high.

*Argon 39*

Argon 39 is produced in the atmosphere by cosmic rays like radiocarbon. As it is a noble gas, the distribution in the sea is by no means affected by any chemical processes. The model treats the mixing ratio $^{39}A/^{40}A$ like the preindustrial radiocarbon in the work by Toggweiler et al. [1989]. The air-sea gas exchange is so quick that the surface values can be assumed to be horizontally homogeneous at a saturation level. The details of the solubility [Weiss, 1970] play, thus, no role. Due to its much shorter lifetime as compared with radiocarbon (400 to 8267 years), the structures in the deep ocean are different from $\Delta^{14}C$. Up to now, there are too few measurements of this tracer [Loosli, 1989] to produce reliable maps of the distribution. Figure 13 shows the covariation of $^{39}A$ with $\Delta^{14}C$ in the deep ocean below one km. The structure of the scatter indicates the relative importance of diffusion and advection for the model's tracer distribution: The solution of the one - dimensional advection equation for a decaying tracer

$$\lambda T + uT_x = 0$$

is solved by $T \sim \exp(-\lambda x/u)$, whereas the diffusion equation

$$\lambda T = D\, T_{xx}$$

is solved by $T \sim \exp(-x\ (\lambda/D)^{1/2})$. The theoretical covariation between $^{39}A$ and $^{14}C$ with decay constants $\lambda_a$ and $\lambda_c$ would, thus, be

$$^{39}A = (^{14}C)^{\lambda a/\lambda c}$$

for pure advection, and

$$^{39}A = (^{14}C)^{\sqrt{\lambda a/\lambda c}}$$

19449224, 1993, 3, Downloaded from https://agupubs.onlinelibrary.wiley.com/doi/10.1029/93GB01355 by MPI 348 Meteorology, Wiley Online Library on [11/01/2023]. See the Terms and Conditions (https://onlinelibrary.wiley.com/terms-and-conditions) on Wiley Online Library for rules of use; OA articles are governed by the applicable Creative Commons License

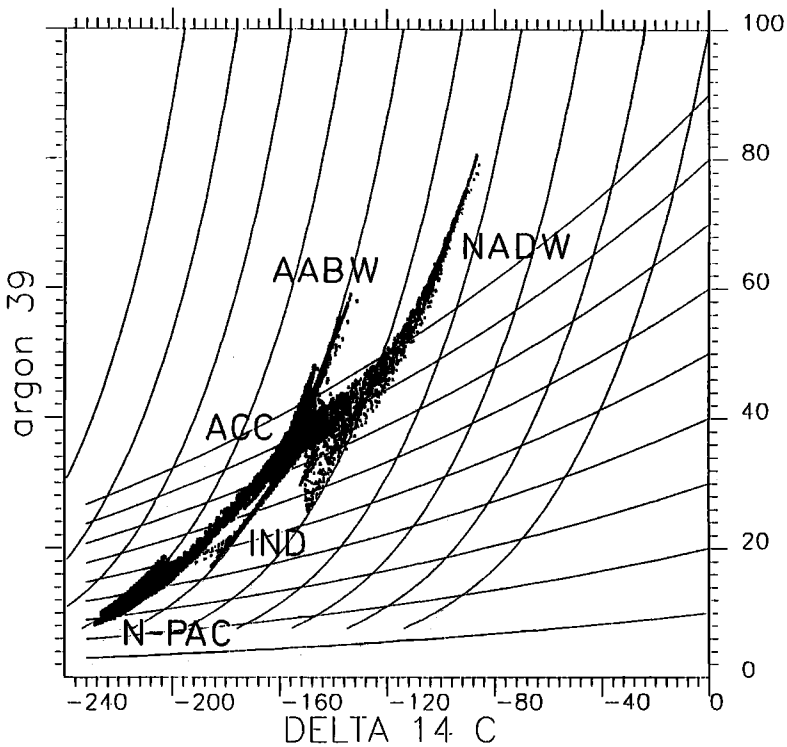


Fig. 13. Scatter of Argon 39 versus $\Delta^{14}C$ in the deep ocean below one km. The lines with steep slope indicate the theoretical advective aging for source waters with different radiocarbon content. The lines with flat slope indicate the same for exclusive diffusion.

for pure diffusion. The scatter is dominated by the slope of the advective decay lines, most pronounced in the Indian ocean and in the upper part of the old Pacific water. In the Antarctic Circumpolar Current, the slope of the scatter is more parallel to the lines of mixing decay.

*The Equatorial Upwelling*

In the eastern equatorial Pacific the model produces unrealistic structures. Too much production is linked with a too weak high of the surface partial pressure of CO2. The flaw is reflected most clearly in the distribution of POC which is not remineralized due to the oxygen deficiency. In the experiment described here, the global inventory of POC is 119 Gt C. The extreme value of 300 μ mol/L is in the Gulf of Panama in 800 m depth. Figure 14a shows the model distribution of phosphate in this depth, whereas Figure 14b displays the distribution of total phosphorus, i.e., the sum of dissolved phosphate and the phosphorus content of particulate matter. The figure resembles remarkably the distribution of phosphate in the S1 experiment by Najjar et al. [1992] shown in Figure 15, where the experiment of Figure 15b is directly comparable to the model of this paper. The maximum can be diminished by the assumption of a large pool of DOC (Figure 15 of their paper) but it has been demonstrated [Bacastow and Maier-Reimer, 1991] that such a "repair" of the phosphate distribution is linked with an underestimate of the global gradients of $\delta^{13}C$. Another explanation could be the neglect of unidentified important processes. It could be apatite formation [Atlas and Pytkowitz, 1977] whose solubility product is very near to 3 μ mol/L of phosphate. It would remove phosphate from the equatorial region which should then be replaced from the continents. Also, the rigorous application of a globally uniform penetration profile may be inappropriate at locations were the model already has an unrealistic state. I ran experiments with the assumption that POC sinks with a moderate velocity through

19449224, 1993, 3, Downloaded from https://agupubs.onlinelibrary.wiley.com/doi/10.1029/93GB01355 by MPI 348 Meteorology, Wiley Online Library on [11/01/2023]. See the Terms and Conditions (https://onlinelibrary.wiley.com/terms-and-conditions) on Wiley Online Library for rules of use; OA articles are governed by the applicable Creative Commons License

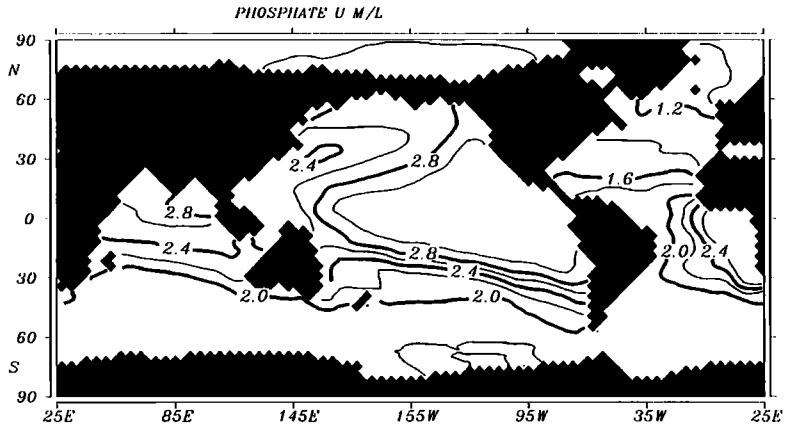


Fig. 14a. dissolved phosphate in 800 m depth, the horizon of maximum POC.

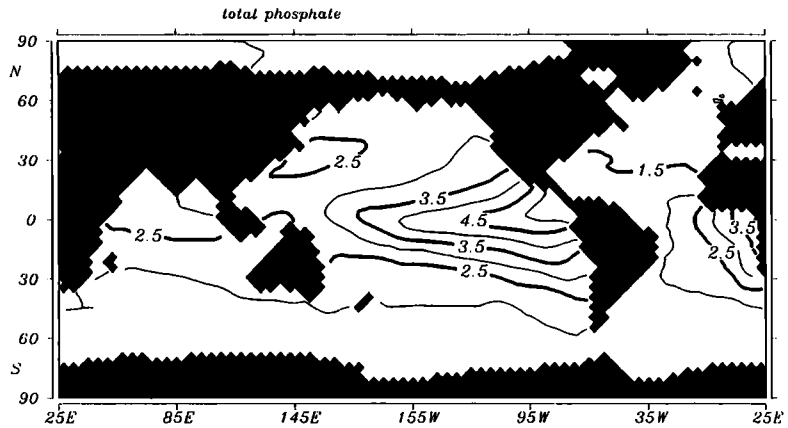


Fig. 14b. Sum of dissolved and particulate phosphate.

regions with strong oxygen deficits. In these experiments, the problem was shifted to the bottom, yielding there a pronounced minimum of oxygen and maximum of phosphate, distributed over a larger volume.

A more definite restriction of the model is the neglect of details of the plankton dynamics. From the Coastal Zone Color Scanner of the NASA's Nimbus 7 research satellite, beautiful color photographs have been constructed from the distribution of chlorophyll in the ocean [Feldman et al., 1989]. One of the most striking features in these imageries is the weak activity in equatorial regions. We have preliminary indications that the implementation of a Fasham type plankton model serves to reduce substantially the apparent flaws of HAMOCC 3 (K.D. Kurz, personal communication, 1993). The zooplankton community provides a delay between nutrient transormation and particle release during which phosphorus is removed from the equator by surface currents.

It seems, however, possible, too, that the physical circulation models, on which the geochemical models are based, react similarly with too much upwelling on the prescribed windfield, perhaps as a consequence of the coarse vertical resolution of the models.

## 4. CONCLUSION

The model reproduces realistic patterns of global biogeochemical tracer distributions without any restoring to prescribed boundary conditions.

The assumption of an overall constant Redfield ratio appears to be sufficient for modelling the large structures of the tracer distributions.

The model has sufficient degrees of freedom to give information on its weaknesses from its own. Further steps of model development will include higher resolution and a more realistic treatment of important (to the carbon cycle)

19449224, 1993, 3, Downloaded from https://agupubs.onlinelibrary.wiley.com/doi/10.1029/93GB01355 by MPI 348 Meteorology, Wiley Online Library on [11/01/2023]. See the Terms and Conditions (https://onlinelibrary.wiley.com/terms-and-conditions) on Wiley Online Library for rules of use; OA articles are governed by the applicable Creative Commons License

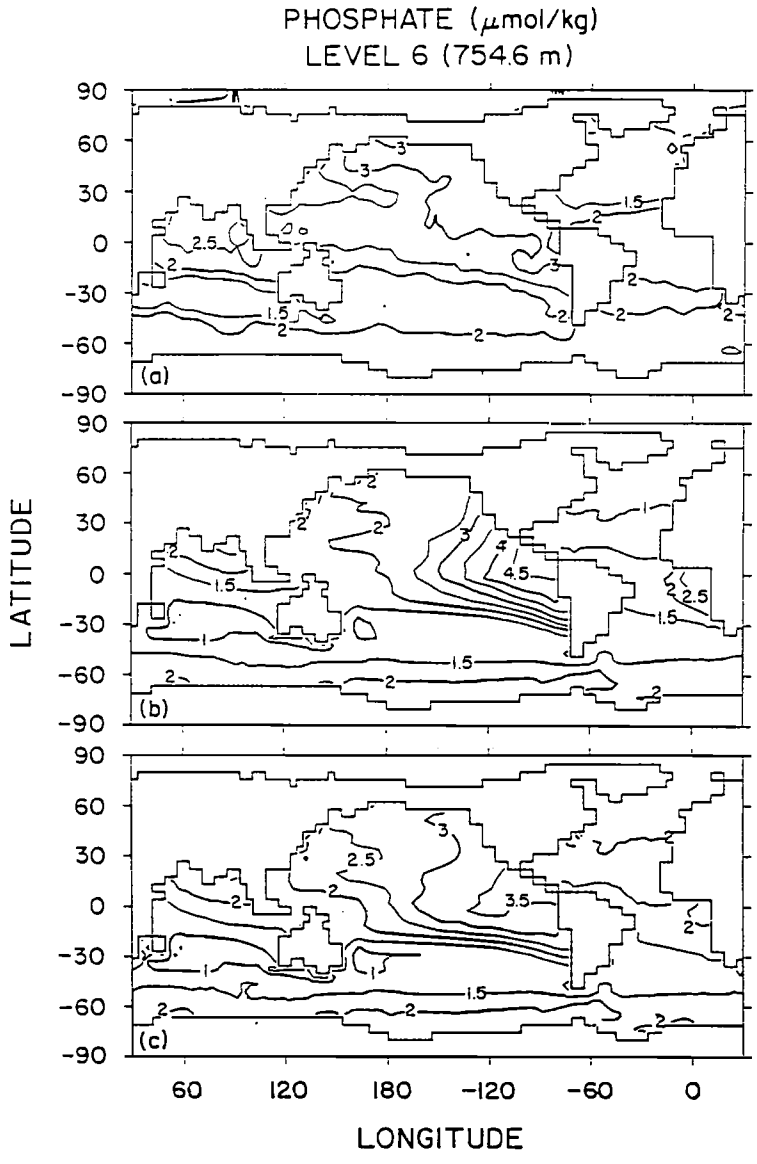


Fig. 15. From Najjar et al. [1992]. (a) Phosphate from observations. (b) with penetration of particulate matter according $z^{-0.858}$. (c) with penetration according exp(-z/800m).

biological processes. We will try to keep the model as simple as possible with only few free parameters in order to retain the principal predictive power in the coupling to climate models.

## APPENDIX: TECHNICAL DETAILS

### *Advection*

Tracer conservation is the only rigorous constraint for the model. The model uses a staggered grid, where the locations of velocity points are in all three dimensions halfway between the tracer points. By defining the tracer inventory $CI = \Sigma V_k C_k$ for any tracer C, the advection equation is written:

$$V(C - C^{old})/\Delta t = \sum_{i=1}^{3} T_{i-1/2}(C_{i-1} + C) - T_{i+1/2}(C_{i+1} + C) + |T_{i-1/2}|(C_{i-1} - C) + |T_{i+1/2}|(C_{i+1} - C)$$

where T is half the transport of water that enters or leaves the grid cell. The first two terms on the right hand side represent a direct difference of advective fluxes,

19449224, 1993, 3, Downloaded from https://agupubs.onlinelibrary.wiley.com/doi/10.1029/93GB01355 by MPI 348 Meteorology, Wiley Online Library on [11/01/2023]. See the Terms and Conditions (https://onlinelibrary.wiley.com/terms-and-conditions) on Wiley Online Library for rules of use; OA articles are governed by the applicable Creative Commons License

whereas the third and fourth term stand for the divergence of diffusive fluxes. The system determines all values of C simultaneously; it is solved by iteration. After four iterations, the approximative solution $C^*$ is sufficiently precise to allow a direct insertion of $C^*$ in the right hand side of the system, which guarantees tracer conservation. A reordering of the various terms shows that the system links for every grid cell the incoming tracer transports with the outgoing water transports. In the interior ocean, water continuity is exactly preserved by the currents. In the surface layer, however, the tracers are subject to dilution or concentration depending on the local freshwater flux. (In the LSG circulation model, the restoring to surface salinity is realized by direct variations of sealevel, preserving total salt. This yields small divergences of the surface currents.) This mechanism drives the tracer gradients to follow those of salinity. It is seen most clearly in the surface alkalinity.

### Gas Exchange

With $s = [CO_2]$ and $h = [H^+]$, we have

$$\Sigma CO = s(1+K_1/h + K_1K_2/h^2), \text{ and}$$

$$Alk = s(K_1/h+2K_1K_2/h^2)+B_T/(1+h/K_B)+K_W/h - h$$

$$= \Sigma CO_2(K_1/h + 2K_1K_2/h^2)/(1+K_1/h +K_1K_2/h^2)$$

$$+ B_T/(1+h/K_B)+K_W/h-h.$$

in the usual notation for dissociation constants and the aqueous and borate system [cf. Dickson, 1981]. The latter expression contains h as the only unknown for the determination of the system at given $\Sigma CO_2$ and Alk. It is easily found by a Newton iteration. With the geometrical capacities M of atmosphere and ocean boxes, the gas exchange is written

$$M_o(\Sigma CO_2^{new} - \Sigma CO_2^{old}) = \frac{k\,\Delta t}{2}$$

$$\{ (P_a - p(Alk,\Sigma CO_2)^{old}+(P_a - p(Alk,\Sigma CO_2)^{new}\}$$

and

$$M_a(p_a^{new} - p_a^{old}) = - \frac{k\,\Delta t}{2}$$

$$\{ (P_a - p(Alk,\Sigma CO_2)^{old}+(P_a - p(Alk,\Sigma CO_2)^{new}\},$$

where $p_a$ is the atmospheric $pCO_2$ and $p(Alk,\Sigma CO_2)$ is the oceanic partial pressure, to be obtained from the Newton iteration, and k is the gas exchange coefficient modified by the solubility. This rather complicated scheme is taken from HAMOCC 2 with the time step of one year. For the experiment with a constant gas exchange coefficient, it provides a superfluous degree of accuracy. In experiments with variable gas exchange coefficients, however, the modifications by the semi-implicit scheme become noticeable around Antarctica.

*Acknowledgements.* I am deeply indebted to Wallace Broecker, who has guided me during the past years with his well balanced mixture of rigorous criticism and enthusiastic encouragement. I appreciated the cooperation with R.Bacastow in developing the main framework of the model. For fruitful discussions thanks are to, inter al., D. Archer, M. Bender, W. Berger, A. Björkström, B. Bolin, H. C. Broecker, U. Brockmann, E. Degens, J. C. Duplessy, K. Hasselmann, M. Heimann, C. Heinze, K. Holmen, K. Kurz, V. Ittekott, S. Kempe, W. Roether, J. Sarmiento, M. Sarnthein, N. Shackleton, A. Spitzy, R. Toggweiler, and three more or less anonymous reviewers. The work was supported by EC contract CT900017.

### REFERENCES

Archer, D., Modelling the calcite lysocline, *J. Geoph. Res., 96,* C9, 17037-17050, 1991.

Atlas, E., and R. M. Pytkowicz,Solubility behavior of apatite in seawater, *Limnol. Oceanogr., 22,* 290-300, 1977.

Bacastow, R., and E. Maier-Reimer, Ocean-circulation model of the carbon cycle, *Clim. Dyn., 4,* 95-125, 1990.

Bacastow, R., and E.Maier-Reimer, Dissolved organic carbon in modeling oceanic new production, *Global Biogeochem. Cycles, 5,* 71-85, 1991.

Bainbridge, A., *GEOSECS Atlantic Expedition,* Sections and profiles, Washington, D.C., 1980.

Bender, M. L., The $\delta^{18}O$ of dissolved $O_2$ in seawater: A unique tracer of circulation and respiration in the deep sea, *J. Geophys. Res.,95,* 22243 - 22252, 1990.

Berger, W. H., K. Fischer, C. Lai, and G. Wu, Ocean productivity and organic carbon flux, Part I, Overview of maps of primary production and export production, *SIO Ref. 87-30,* Univ. of Calif., San Diego, 1987.

Bolin, B. (Ed.), *Carbon Cycle Modelling,* 390 pp., John Wiley, New York, 1982.

Broecker, W. S., and T. Takahashi, The relationship between lysocline depth and

19449224, 1993, 3, Downloaded from https://agupubs.onlinelibrary.wiley.com/doi/10.1029/93GB01355 by MPI 348 Meteorology, Wiley Online Library on [11/01/2023]. See the Terms and Conditions (https://onlinelibrary.wiley.com/terms-and-conditions) on Wiley Online Library for rules of use; OA articles are governed by the applicable Creative Commons License

in situ carbonate ion concentration, *Deep Sea Res., 25,* 65 - 95, 1978.

Broecker, W. S., and T. H. Peng, *Tracers in the Sea,* 691 pp., Eldigio, Palisades, 1982.

Broecker, W. S., and E. Maier-Reimer, The influence of air and sea exchange on the carbon isotope distribution in the sea, *Global Biogeochem. Cycles, 6,* 315-320, 1992.

Broecker, W. S., T. H. Peng, G. Östlund, and M. Stuiver, The distribution of bomb radiocarbon in the ocean, *J. Geophys. Res., 90,* 6953-6970, 1985.

Broecker, W.S., S. Blanton, W. M. Smethie, and G. Östlund, Radiocarbon decay and oxygen utilization in the deep Atlantic Ocean, *Global Biogeochem. Cycles, 5,* 87-117, 1991.

Bryan, K., A numerical method for the study of the circulation of the World Ocean, *J. Comput. Phys., 4,* 437-376, 1969.

Craig, H., and P. Kroopnick, Oxygen-18 variations in dissolved oxygen in the sea (abstract), *Eos Trans. AGU,* 51, 325, 1970.

Craig, H., W. S. Broecker, and D. Spencer, *GEOSECS Pacific Expedition,* Sections and profiles, National Science Foundation, Washington, D. C., 1981.

Culberson, C. H. and R. M. Pytkowicz, Effect of pressure on carbonic acid, boric acid and th pH in sea water, *Limnol. Oceanogr., 13,* 403-417, 1968

Degens, E. T., S. Kempe and A. Spitzy, Carbon dioxide: A biogeochemical portrait, in, *The Handbook of Environmental Chemistry,* Vol. 1/Part C, O. Hutzinger, pp. 127-215, Springer, Berlin Heidelberg, 1984.

Dickson, A. G., An exact definition of total alkalinity and a procedure for the estimation of alkalinity and total inorganic carbon from titration data, *Deep Sea Res., Part A, 28,* 609-623, 1981.

Dugdale, R.C., Nutrient limitation in the sea: Dynamics, identification, and significance, *Limnol. Oceanogr., 12,* 685-695, 1967.

Dymond, J., and M. Lyle, Flux comparisons between sediments and sediment traps in the eastern tropical Pacific: Implications for $CO_2$ variations during the Pleistocene, *Limnol. and Oceanogr., 30,* 699-712, 1985.

Edmond, J. M., and J. M. T. M. Gieskes, On the calculation of the degree of saturation in sea water with respect to calcium carbonate under in situ conditions, *Geochim. Cosmochim. Acta, 34,* 1261-1291, 1970.

Eppley, R. W., J. N. Rogers, and J. J. McCarthy, Half saturation constants for uptake of nitrate and ammonium by marine phytoplankton, *Limnol. Oceanogr., 14,* 912-920, 1969.

Fasham, M. J. R., H. W. Ducklow, and S.M. McKelvie, A nitrogen-based model of plankton dynamics in the oceanic mixed layer, *J. Mar. Res., 48,* 591-639, 1990.

Feldman, G. C., et al., Ocean color: Availability of the global data set. *Eos Trans. AGU, 70,* 634-641, 1989.

Goyet, C., and A. Poisson, New determination of carbonic acid dissociation constants in seawater as a function of temperature and salinity, *Deep Sea Res., 36,* 1635-1654, 1989.

Heinze, C., E. Maier-Reimer, and K. Winn, Glacial $pCO_2$ reduction by the World Ocean: Experiments with the Hamburg carbon cycle model, *Paleoceanography, 6,* 395-430, 1991.

Houghton, J. T., G. J. Jenkins, and J.J. Ephraums, *Climate Change, The IPCC Scientific Assessment,* 365 pp., Cambridge University Press, New York, 1990.

Keeling, C. D., Carbon dioxide in surface waters, 4, Global distribution, *J. Geophys. Res., 73,* 4543-4553, 1968.

Keeling, C. D., S. C. Piper, and M. Heimann, A three dimensional model of atmospheric $CO_2$ transport based on observed winds, 4. Mean annual gradients and interannual variations, in *Aspects of Climate variability in the Pacific and the Western Americas, Geophys. Monogr. Ser.,* vol. 55, edited by D. H. Peterson, pp. 305-363, AGU, Washington, D. C., 1989.

Koblents-Mishke, O. L., Primary production, in *Oceanology. Biology of the Ocean,* (in Russian), vol. 1, edited by M. E. Vinogradov, pp. 86 - 97, Nauka, Moscow, 1967.

Kroopnick, P. M., The distribution of $\delta^{13}C$ of $\Sigma CO_2$ in the world oceans. *Deep Sea Res., 32,* 57-84, 1985.

Kroopnick, P. M., Oxygen 18 in dissolved oxygen, in *GEOSECS Atlantic, Pacific and Indian Ocean Expeditions,* vol. 7, *Shorebased Data and Graphics,* edited by H. G. Östlund, H. Craig, W. S. Broecker, and D. Spencer, pp. 3 and 27-182, U.S. Government Printing Office, Washington, D. C., 1987.

Kurz, K. D., and E. Maier-Reimer, Iron fertilization in the Austral Ocean - the Hamburg model assessment, *Global Biogeochem. Cycles, 7,* 229-244, 1993.

Levitus, S., Climatological Atlas of the World Ocean, Prof. Pap. 13, National Oceanic and Atmospheric Administration, Rockville, Md., 1982.

19449224, 1993, 3, Downloaded from https://agupubs.onlinelibrary.wiley.com/doi/10.1029/93GB01355 by MPI 348 Meteorology, Wiley Online Library on [11/01/2023]. See the Terms and Conditions (https://onlinelibrary.wiley.com/terms-and-conditions) on Wiley Online Library for rules of use; OA articles are governed by the applicable Creative Commons License

Lisitzin, A. P., Distribution of carbonate microfossils in suspension and in bottom sediments, in *The micropaleontology of Oceans,* edited by B. M. Funnell and W. R. Riedel,Cambridge University Press, pp. 197-218, New York, 1971.

Liss, P. S., and L. Merlivat, Air-Sea gas exchange rates: Introduction and Synthesis, in *The Role of Air-Sea Exchange in Geochemical Cycling,* edited by P. Buat-Menard, pp. 113-127, D. Reidel, Hingham, Mass., 1986.

Loosli, H. H., $^{39}$Ar: A tool to investigate ocean water circulation and mixing, in *Handbook of Environmental Isotope Chemistry,* Vol. 3, *The Marine Environment,* edited by P. Fritz and J. C. Fontes, pp. 385-392. Elsevier, New York, 1989.

Maier-Reimer, E., and K. Hasselmann, Transport and storage of CO2 in the ocean - An inorganic ocean-circulation carbon cycle model, *Clim. Dyn. 2,* 63-90, 1987.

Maier-Reimer, E., and R. Bacastow, Modelling of geochemical tracers in the ocean, in *Climate-Ocean Interaction,* edited by M. Schlesinger, pp. 233-267, Kluwer Academic, Boston, Mass., 1990.

Maier-Reimer, E., U. Mikolajewicz, and K. Hasselmann, Mean Circulation of the Hamburg LSG OGCM and its sensitivity to the thermohaline surface forcing, *J. Phys. Oceanogr., 23,* 731-757, 1993.

Martin, J. H., R. M. Gordon, and S. E. Fitzwater, Iron in Antarctic waters, *Nature, 345,* 156-158, 1990.

Mook, W. G., J. C. Bommerson, and W. H. Staverman, Carbon isotope fractionation between dissolved bicarbonate and gaseous carbon dioxide, *Earth Planet. Sci. Lett., 22,* 169-176, 1974.

Najjar, R. G., Simulations of the phosphorus and oxygen cycles in the world ocean using a general circulation model, Ph.D. thesis, Princeton Univ., Princeton, N. J. 1990.

Najjar, R. G., J. L. Sarmiento, and J. R. Toggweiler, Downward transport and fate of organic matter in the ocean: Simulations with a general circulation model, *Global Biogeochem. Cycles, 6,* 45-76, 1992.

Oeschger, H., U. Siegenthaler, U. Schotterer, and A. Gugelmann, A box diffusion model to study the carbon dioxide exchange in nature, *Tellus, 27,* 168-192, 1975.

Peng, T. H., W. S. Broecker, H. D. Freyer, and S. Trumbore: A convolution of the tree-ring based δ 13C record, *J. Geophys. Res., 88,* 3609-3620, 1983.

Radach, G. and E. Maier-Reimer, The vertical structure of phytoplankton growth dynamics - A mathematical model, *Mem. Soc. Roy. Sci. Liege, 7,* 6e Ser., 113-146, 1975.

Rau, G. H., P. N. Froelich, T. Takahashi, and D. J. Des Marais, Does sedimentary organic $\delta^{13}C$ record variations in Quaternary Ocean [ΣCO2(aq)]?, *Paleoceanography, 6,* 335-347, 1991.

Revelle, R. and H. E. Suess, Carbon dioxide exchange between atmosphere and ocean and the question of an increase of atmospheric CO2 during the past decades, *Tellus, 9,* 18-27, 1957.

Sarmiento, J. L., and J. C. Orr, Three-dimensional simulations of the impact of Southern Ocean nutrient depletion on atmospheric CO2 and ocean chemistry, *Limnol. Oceanogr., 38,* 1928-1950, 1991.

Sarmiento, J. L., J. C. Orr, and U. Siegenthaler, A perturbation simulation of CO2 uptake in an ocean general circulation model, *J. Geophys. Res., 97,* 3621-3646, 1992.

Schlesser, G. H., Oxygen isotope fractionation during respiration for different temperatures of T. utilis and E.coli K12, *Radiat. Environ. Biophys., 17,* 85-93, 1979.

Siegenthaler, U., Uptake of excess CO2 by an outcrop-diffusion model of the ocean, *J. Geophys. Res., 88,* 3599-3608, 1983.

Suess, E., Particulate organic carbon flux in the oceans - Surface productivity and oxygen utilization, *Nature, 288,* 260-263, 1980.

Sugimura, Y., and Y. Suzuki, A high-temperature catalytic oxidation method for the determination of non-volatile dissolved organic carbon in seawater by direct injection of a liquid sample, *Mar. Chem., 24,* 105-131, 1988.

Suzuki, Y., On the measurement of DOC and DON in seawater, *Mar. Chem., 41,* 287-288, 1993.

Takahashi, T., W. S. Broecker, and S. Langer, Redfield ratio estimates based on chemical data from isopycnal surfaces, *J. Geophys. Res., 90,* 5907-5924, 1985.

Takahashi, T., D. Chipman, and T. Volk, Geographical, seasonal, and secular variations of the partial pressure of CO2 in surface waters of the North Atlantic Ocean: The results of the North Atlantic TTO program, in *Proceedings of Carbon Dioxide Research Conference: Carbon Dioxide, Science and Consensus,* CONF 820970 U.S. Department of Energy, Washington, D. C., 1983

19449224, 1993, 3, Downloaded from https://agupubs.onlinelibrary.wiley.com/doi/10.1029/93GB01355 by MPI 348 Meteorology, Wiley Online Library on [11/01/2023]. See the Terms and Conditions (https://onlinelibrary.wiley.com/terms-and-conditions) on Wiley Online Library for rules of use; OA articles are governed by the applicable Creative Commons License

Tans, P. P., I. Y. Fung, and T. Takahashi, Observational constraints on the global atmospheric CO2 budget, *Science, 247,* 1431-1438, 1990.

Toggweiler, J. R., K. Dixon and K Bryan, Simulations of radiocarbon in a coarse-resolution wWorld ocean model, I, steady state prebomb distributions, *J. Geophys. Res., 94,* 8217-8242, 1989.

Tsunogai, S., and S. Noriki, Particulate fluxes of carbonate and organic carbon in the ocean. Is the marine biological activity working as a sink of the atmospheric carbon?, *Tellus, Ser. B, 43,* 256-266, 1991.

Weiss, R. F., Carbon dioxide in water and sea water: The solubility of a nonideal gas, *Mar. Chem. 2,* 203-215, 1974.

Weiss, R. F. The solubility of nitrogen, oxygen, and argon in water and sea water. *Deep Sea Res., 17,* 721-735, 1970.

Williams, P. M., and E. R. M. Druffel, Radiocarbon in dissolved organic matter in the central North Pacific Ocean, *Nature, 330,* 246-248, 1987.

Woodruff, S. D., R. J. Slutz, R. L. Jenne, and P.M. Steurer, A comprehensive ocean-atmosphere data set, *Bull. Am. Meteorol. Soc., 68,* 1239-1250, 1987.

---

E. Maier-Reimer, Max Planck Institut fuer Meteorologie, Bundesstrasse 55, 20146 Hamburg, Germany.

(Received February 18, 1993;
revised May 13, 1993;
accepted May 21, 1993.)

19449224, 1993, 3, Downloaded from https://agupubs.onlinelibrary.wiley.com/doi/10.1029/93GB01355 by MPI 348 Meteorology, Wiley Online Library on [11/01/2023]. See the Terms and Conditions (https://onlinelibrary.wiley.com/terms-and-conditions) on Wiley Online Library for rules of use; OA articles are governed by the applicable Creative Commons License